Monthly Notices
of the
ROYAL ASTRONOMICAL SOCIETY

Mon. Not. R. Astron. Soc. **424,** 801–819 (2012) doi:10.1111/j.1365-2966.2012.20634.x

# Cosmological measurements with forthcoming radio continuum surveys

Alvise Raccanelli,[1⋆] Gong-Bo Zhao,[1] David J. Bacon,[1] Matt J. Jarvis,[2,3] Will J. Percival,[1] Ray P. Norris,[4] Huub Röttgering,[5] Filipe B. Abdalla,[6] Catherine M. Cress,[3,7] Jean-Claude Kubwimana,[8] Sam Lindsay,[2] Robert C. Nichol,[1] Mario G. Santos[9] and Dominik J. Schwarz[10]

[1]*Institute of Cosmology and Gravitation, University of Portsmouth, Dennis Sciama Building, Portsmouth, P01 3FX*
[2]*Centre for Astrophysics Research, STRI, University of Hertfordshire, Hatfield, AL10 9AB*
[3]*Physics Department, University of the Western Cape, Bellville 7535, South Africa*
[4]*CSIRO Astronomy and Space Science, PO Box 76, Epping, NSW 1710, Australia*
[5]*Leiden Observatory, Leiden University, PO Box 9513, NL-2300 RA Leiden, the Netherlands*
[6]*Department of Physics and Astronomy, University College London, Gower Street, London, WC1E 6BT*
[7]*Centre for High Performance Computing, 15 Lower Hope St, Cape Town 7700, South Africa*
[8]*Institut de Recherche en Astrophysique et Planétologie, 9, Av du Colonel Roche, BP 44346, 31028, Toulouse, France*
[9]*CENTRA, Instituto Superior Tecnico, Technical University of Lisbon, Lisboa 1049-001, Portugal*
[10]*Fakultät für Physik, Universität Bielefeld, Postfach 100131, 33501 Bielefeld, Germany*

Accepted 2012 January 25. Received 2012 January 24; in original form 2011 August 3

**ABSTRACT**

We present forecasts for constraints on cosmological models that can be obtained using the forthcoming radio continuum surveys: the wide surveys with the Low Frequency Array (LOFAR) for radio astronomy, the Australian Square Kilometre Array Pathfinder (ASKAP) and the Westerbork Observations of the Deep Apertif Northern Sky (WODAN). We use simulated catalogues that are appropriate to the planned surveys in order to predict measurements obtained with the source autocorrelation, the cross-correlation between radio sources and cosmic microwave background (CMB) maps (the integrated Sachs–Wolfe effect), the cross-correlation of radio sources with foreground objects resulting from cosmic magnification, and a joint analysis together with the CMB power spectrum and supernovae (SNe). We show that near-future radio surveys will bring complementary measurements to other experiments, probing different cosmological volumes and having different systematics. Our results show that the unprecedented sky coverage of these surveys combined should provide the most significant measurement yet of the integrated Sachs–Wolfe effect. In addition, we show that the use of the integrated Sachs–Wolfe effect will significantly tighten the constraints on modified gravity parameters, while the best measurements of dark energy models will come from galaxy autocorrelation function analyses. Using a combination of the Evolutionary Map of the Universe (EMU) and WODAN to provide a full-sky survey, it will be possible to measure the dark energy parameters with an uncertainty of $\{\sigma(w_0) = 0.05, \sigma(w_a) = 0.12\}$ and the modified gravity parameters $\{\sigma(\eta_0) = 0.10, \sigma(\mu_0) = 0.05\}$, assuming *Planck* CMB+SN (current data) priors. Finally, we show that radio surveys would detect a primordial non-Gaussianity of $f_{\rm NL} = 8$ at $1\sigma$, and we briefly discuss other promising probes.

**Key words:** cosmological parameters – cosmology: observations – large-scale structure of Universe – radio continuum: galaxies.

## 1 INTRODUCTION

Radio surveys for cosmology are entering a new phase with the construction of the Low Frequency Array (LOFAR) for radio astronomy (Röttgering 2003), the Australian Square Kilometre Array Pathfinder (ASKAP; Johnston et al. 2008) and Apertif, the new phased array feed receiver system for the Westerbork Synthesis Radio Telescope (WSRT; Oosterloo, Verheijen & van Cappellen 2010). In each case, the increased sensitivity available, together with a very wide sky coverage, will allow certain cosmological statistics to be measured with substantial accuracy. Several studies in the past

⋆E-mail: alvise.raccanelli@port.ac.uk

have concentrated on the cosmological constraints that can be determined from large redshift surveys using the H I 21-cm emission line (e.g. Abdalla & Rawlings 2005; Abdalla, Blake & Rawlings 2010). However, little attention has been paid to the information that can be gleaned from large radio continuum surveys. In many respects, these will be much easier to interpret than the H I surveys and they will allow us to push out to much higher redshifts. In this paper, we consider three experiments using the deep continuum observations: the autocorrelation of radio sources, the cross-correlation of radio sources with the cosmic microwave background (CMB) – the late integrated Sachs–Wolfe (ISW) effect – and the cross-correlation of radio sources with foreground objects (magnification bias). The key issues that we wish to address here are the level of accuracy of these measurements and the relative significance of the various potential probes.

One of the goals of these measurements is to measure the cosmological parameters of particular current interest. Among the biggest challenges in cosmology is to determine whether the standard $\Lambda$ cold dark matter (CDM) model and its general relativity (GR) context are correct, or whether we need a different cosmological model and/or gravitational theory, with the related important implications for fundamental physics. Thus, we present forecasts of the constraints on cosmological models and gravitational parameters that it will be possible to obtain with the LOFAR (Röttgering et al. 2012), ASKAP (Johnston et al. 2008) and WSRT (Oosterloo et al. 2010) radio telescopes, both in isolation and together.

There are many major optical and near-infrared galaxy surveys that aim to improve the precision of cosmological parameter measurements during this decade, for example, the Baryon Oscillation Spectroscopic Survey (BOSS; Eisenstein et al. 2011), BigBOSS (Schlegel et al. 2011), the Dark Energy Survey[1] (DES), the Panoramic Survey Telescope and Rapid Response System[2] (Pan-STARRS), Euclid (Laureijs 2009) and the Large Synoptic Survey Telescope[3] (LSST). One of the goals of this paper is to discover whether there are also significant and complementary opportunities for the improvement of cosmological constraints using forthcoming radio continuum surveys. These surveys have a particular niche because of their large sky coverage, high median redshift and the number of objects observed.

The paper is organized as follows. In Section 2, we describe the next generation of radio surveys. In Section 3, we discuss the predictions for source densities and bias as a function of redshift for each survey and for different source populations. In Section 4, we present the cosmological probes that we will use, and in Section 5, we show our predicted cosmological measurements. In Section 6, we describe the methodology used to predict the resulting constraints on dark energy and modified gravity models, and we present our results in Section 7. In Section 8, we present our conclusions and we summarize why forthcoming radio surveys will be important for cosmology.

## 2 FORTHCOMING RADIO SURVEYS

In this section, first we introduce the three large radio surveys that we focus on in this paper: LOFAR, the Evolutionary Map of the Universe (EMU; a planned survey for ASKAP) and WODAN (a planned survey for the WSRT). Then, we indicate the parameters we have used for our forecasts. We do not consider the surveys to be conducted with the South African SKA Precursor Telescope (MeerKAT; Jonas 2009) because the parameter space probed by MeerKAT is towards much deeper and narrower surveys, which are more adept to studying galaxy formation and evolution. In each case, we discuss the properties of the surveys, and their expected time-scales for observations. A summary of the properties of the surveys is shown in Table 1.

### 2.1 LOFAR

LOFAR (Röttgering et al. 2012) is a multinational telescope that has stations spanning Europe. The core of LOFAR is situated in the north-east of the Netherlands, with stations on longer baselines both within the Netherlands and across to Germany, the UK, France and Sweden. Other stations might also be added throughout the rest of Europe in the coming years.

Each LOFAR station operates at two broad frequency ranges, the high band operating at $120 < \nu < 240$ MHz and the low band operating at $10 < \nu < 80$ MHz. The bulk of the early operations of LOFAR will be dedicated to a number of key science projects (KSPs): Solar Physics and Space Weather, Transients, Cosmic Magnetism, the Epoch of Reionization, Cosmic Rays and Continuum Surveys. It is the last of these that is pertinent to our aims in this paper.

The Continuum Surveys KSP will explore the bulk of the Northern sky at low radio frequencies. Low-frequency radio observations are ideally suited for carrying out sensitive surveys of the extragalactic sky. This is because the low frequency ensures a large instantaneous field of view, which allows an increased survey speed compared to similar telescopes operating at higher frequencies. Also, the bulk of radio emission detected from extragalactic sources is a result of synchrotron radiation, and therefore it increases towards lower frequencies, although at the very lowest frequencies a turnover might be expected to occur because of synchrotron self-absorption.

The LOFAR continuum surveys (Röttgering 2010) follow the usual strategy of a 'wedding cake' tiered survey. The design of these surveys has focused on addressing the original key science topics within the continuum surveys, namely tracing the formation of massive galaxies, clusters and black holes using high-redshift radio sources, measuring the star formation history of the Universe through radio emission and tracing intracluster magnetic fields using diffuse radio emission. However, as we demonstrate, these surveys will also provide key data that can be used to constrain the cosmology and gravitational physics in our Universe.

For the purposes of this paper, we concentrate solely on the 120-MHz surveys from LOFAR, because these are the most sensitive for our science (i.e. wide-field and highly sensitive). The tiers of the LOFAR survey are as follows: the large-area, Tier-1 survey

**Table 1.** Parameters of the surveys considered. We use the $10\sigma$ flux-density limit for each survey. The total number of radio sources $N_{\rm gal}$ and the mean and median redshifts are calculated using our number density models in Section 3.

| Survey | Area | Frequency (MHz) | $N_{\rm gal}$ | Mean $z$ | Median $z$ |
|---|---|---|---|---|---|
| LOFAR MS[3] | $2\pi$ | 150 | $1.0 \times 10^6$ | 1.6 | 1.3 |
| LOFAR Tier1 | $2\pi$ | 120 | $6.5 \times 10^6$ | 1.8 | 1.1 |
| EMU | $3\pi$ | 1400 | $2.2 \times 10^7$ | 1.7 | 1.1 |
| WODAN | $1\pi$ | 1400 | $7.3 \times 10^6$ | 1.7 | 1.1 |

[1] http://www.darkenergysurvey.org/
[2] http://pan-starrs.ifa.hawaii.edu/public/
[3] http://www.lsst.org/lsst

will survey the whole of the Northern sky down to an expected rms flux density at 120 MHz of $S_{120\,\mathrm{MHz}} = 0.1$ mJy.

The LOFAR Tier-2 survey will survey to deeper levels over a smaller area. The baseline strategy is to survey around 550 deg$^2$ at 120 MHz to an rms flux density of $S_{120\,\mathrm{MHz}} = 25$ μJy.

The Tier-3 survey is not considered in this paper because of the relatively small area it will survey ($\sim$70 deg$^2$) at 150 MHz to $\sim$6 μJy rms.

We also consider what results could be achieved with the LOFAR commissioning survey, the Multifrequency Snapshot Sky Survey (MSSS). Although this survey is still being fully defined, we take a shallow survey covering the whole Northern hemisphere at 150 MHz and we use a $10\sigma$ limit of 7 mJy. This allows us to examine what can be achieved with a relatively shallow survey covering 20 000 deg$^2$. We note that the current baseline plan for the commissioning survey is to reach a depth of <5 mJy over the 120–170 MHz band. Thus, our assumed survey is on the optimistic side of what might actually be produced in the final commissioning survey, although as more baselines are added this depth might increase as the survey progresses. However, we note that 5 mJy at 150 MHz is a similar depth to that of the National Radio Astronomy Observatory (NRAO) Very Large Array (VLA) Sky Survey (NVSS) at 1.4 GHz, assuming a spectral index of $\alpha = 0.8$ $S_\nu \propto \nu^{-\alpha}$. Therefore, similar constraints would be expected.

If we assume that only the stations situated in the Netherlands are used to carry out the large-area surveys, then the resolution at 120 MHz will be $\sim$6 arcsec and around $\sim$5 arcsec at 150 MHz, which is very similar to the Faint Images of the Radio Sky at 21-cm (FIRST) survey (Becker, White & Helfand 1995).

### 2.2 Evolutionary Map of the Universe

The EMU (Norris et al. 2011) is an all-sky continuum survey planned for the new ASKAP (Johnston et al. 2008) telescope under construction on the Australian candidate SKA site in Western Australia. The EMU is one of two key projects (the other is the WALLABY all-sky H I survey) that are primarily driving the ASKAP design. At its completion, expected to be in late 2012, ASKAP will consist of 36 12-m antennas spread over a region 6 km in diameter. Although the collecting area is no larger than many existing radio telescopes, the phased array feed at the focus of each antenna provides about 100 dual-polarization pixels, giving ASKAP a 30 deg$^2$ instantaneous field of view. This enables it to survey the sky some 30 times faster than existing radio telescopes at similar frequencies.

The primary goal of the EMU is to make a deep (10 μJy rms) radio continuum survey of the entire Southern sky, extending as far north as +30 deg. The EMU will cover the same area (75 per cent of the sky) as the NVSS (Condon et al. 1998), but it will be 45 times more sensitive, and it will have an angular resolution (10 arcsec) five times better. It will also have higher sensitivity to extended structures. The EMU is expected to begin in late 2012, and it will generate a catalogue of radio sources 38 times larger than NVSS; all radio data from the EMU will be placed in the public domain as soon as the data quality has been checked.

### 2.3 WODAN

WODAN is planned to chart the entire Northern sky above Dec. $>30^\circ$ down to a proposed rms flux density at 1.4 GHz of $S_{1.4\,\mathrm{GHz}} = 10$ μJy beam$^{-1}$ (Röttgering et al. 2012). It will be able to do this because of the new phased array feeds (Apertif) being put on the WSRT (Oosterloo et al. 2010). The phased array feeds will open up the field of view of the WSRT to around 8 deg$^2$, allowing very high survey speeds. Such a survey is extremely complementary to the proposed LOFAR Tier-1 survey, and it will allow source spectral indices to be measured down to very faint levels. Although Apertif increases the field of view of the WSRT considerably, it will remain a relatively low-resolution survey instrument, with the resolution limited to the distribution of the WSRT antennas; as such, the resolution will be around $\sim$15 arcsec. However, this resolution is generally not a problem for the experiments we discuss in this paper. The current schedule for the commencement of the Apertif surveys is 2013.

## 3 SOURCE POPULATION MODELS

In this section, we describe our models for source populations for the LOFAR, EMU and WODAN surveys – in particular, the number density of different source populations as a function of redshift and the bias of different source populations as a function of redshift. These are required in order to make predictions for cosmological probes, such as the autocorrelation function and the cross-correlation of radio sources with the CMB (the ISW effect) and with foreground sources (magnification bias).

### 3.1 Number densities

We use empirical simulations to predict the number density of radio sources per redshift interval for the envisaged all-hemisphere LOFAR survey, the WODAN survey and the ASKAP–EMU 3π steradian (sr) survey. The combination of these surveys will provide complete coverage of 4π sr of the sky; however, the different observing frequencies and depths mean that the surveys will produce distinct redshift distributions, which need to be understood in order to use the combination for cosmological constraints. Throughout this paper, we assume that no redshift information is available for individual radio sources.

We use the simulations of Wilman et al. (2008, 2010), which have been developed for predictions for the SKA continuum survey. These simulations provide specific prescriptions for the redshift evolution of the various populations that dominate the radio-source counts: powerful active galactic nuclei (AGNs) at bright fluxes, down to the less luminous radio-quiet AGNs and starburst and star-forming galaxies. The simulations cover five different radio frequencies: 150, 610, 1400, 4860 and 18 000 MHz. We use the update of the simulated catalogue (Wilman et al. 2010), which has been adjusted to incorporate results from mid- and far-infrared data to provide a better estimate of the starburst and star-forming galaxy populations.

The $N(z)$ from these simulations should, in principle, be modified by redshift-space distortions (Rassat 2009) and magnification bias (Loverde, Hui & Gaztanaga 2007), which are not included. However, these corrections are small and will not affect our results.

The catalogues are generated from the SKA Simulated Skies (S$^3$) data base[4] corresponding to the radio flux-density limits of the proposed LOFAR, EMU and WODAN surveys. As described in Section 2, we assume the depth of the LOFAR survey over the whole hemisphere to be uniform across the sky down to a rms flux-density of 0.1 mJy, as given in the LOFAR survey document Morganti et al. (2009). For the purposes of this paper, we use the 151-MHz data from the S$^3$ data base, and we extrapolate to 120 MHz using the

[4] http://s-cubed.physics.ox.ac.uk

spectral index determined between 610 and 151 MHz to predict the number density distribution. As the simulations include a spectral curvature term, this means that the spectral index between 610 and 151 MHz is generally flatter than the canonical $\alpha \sim 0.7$. Thus, this leads to a decrease in the number of sources expected, based on using $\alpha \sim 0.7$. We adopt these numbers as a conservative approach; however, we note that if the radio spectra do not flatten significantly to low frequencies, then the constraints from LOFAR Tier 1 will be similar to those of the EMU survey, albeit over $2\pi$ sr rather than $3\pi$ sr. We then apply a cut to the simulated data and we retain only those sources with an integrated flux density larger than 10 times the rms noise in the map. Note that for extended sources, the nominal sensitivity to peak flux densities is then less than $10\sigma$. However, this definition ensures that the virtually all extended sources will be detected. It is also conservative in the sense that it still has to be proven that all these new instruments can reach their theoretical thermal noise levels.

For the EMU and WODAN surveys, we again use the Wilman et al. (2008, 2010) simulations, this time at the 1.4-GHz frequency. The EMU will survey ∼75 per cent of the sky down to an rms flux-density limit of 10 μJy, while WODAN will survey 10 000 deg$^2$ down to an rms flux-density limit of 10 μJy. Again, we extract a catalogue from the S$^3$ data base down to this limit and we apply cuts at $10\sigma$ signal-to-noise. Note that Norris et al. (2011) assume a less conservative $5\sigma$ threshold and therefore they obtain stronger constraints.

Figs 1 and 2 show the resulting redshift distributions adopted for the different surveys. In Fig. 1 we display the total number of radio sources for the LOFAR (MS$^3$ and Tier1), EMU and WODAN surveys, while in Fig. 2 we display the number of sources for the different source types within the surveys, that is, star-forming galaxies, starbursts, radio-quiet quasars, Fanaroff–Riley types I and II (FR I and II); see Wilman et al. (2008) for details of how each of these is defined.

In addition to predictions for the four surveys considered, we also consider a combination of EMU and WODAN, given that these surveys will span a similar range of frequencies and depths (see Table 1), in order to have a complete full-sky catalogue covering both hemispheres.

### 3.2 Galaxy bias

As we will often be using radio sources as a probe of large-scale structure (LSS), it is necessary to model how biased the sources are in relation to the underlying structures. On large scales, we assume that the two-point correlation function can be written (Matarrese et al. 1997; Moscardini et al. 1998) as

$$\xi(r, z) = b^2(M_{\rm eff}, z)\xi_{\rm DM}(r, z), \quad (1)$$

where $M_{\rm eff}$ represents the effective mass of dark matter haloes in which sources reside and $\xi_{DM}$ is the correlation function of dark matter. We derive a model of the bias using the peak-background split formalism (Cole & Kaiser 1989; Mo & White 1996), following the prescription of Sheth & Tormen (1999); in this context, the mass function of haloes, altered from Press & Schechter (1974), is given

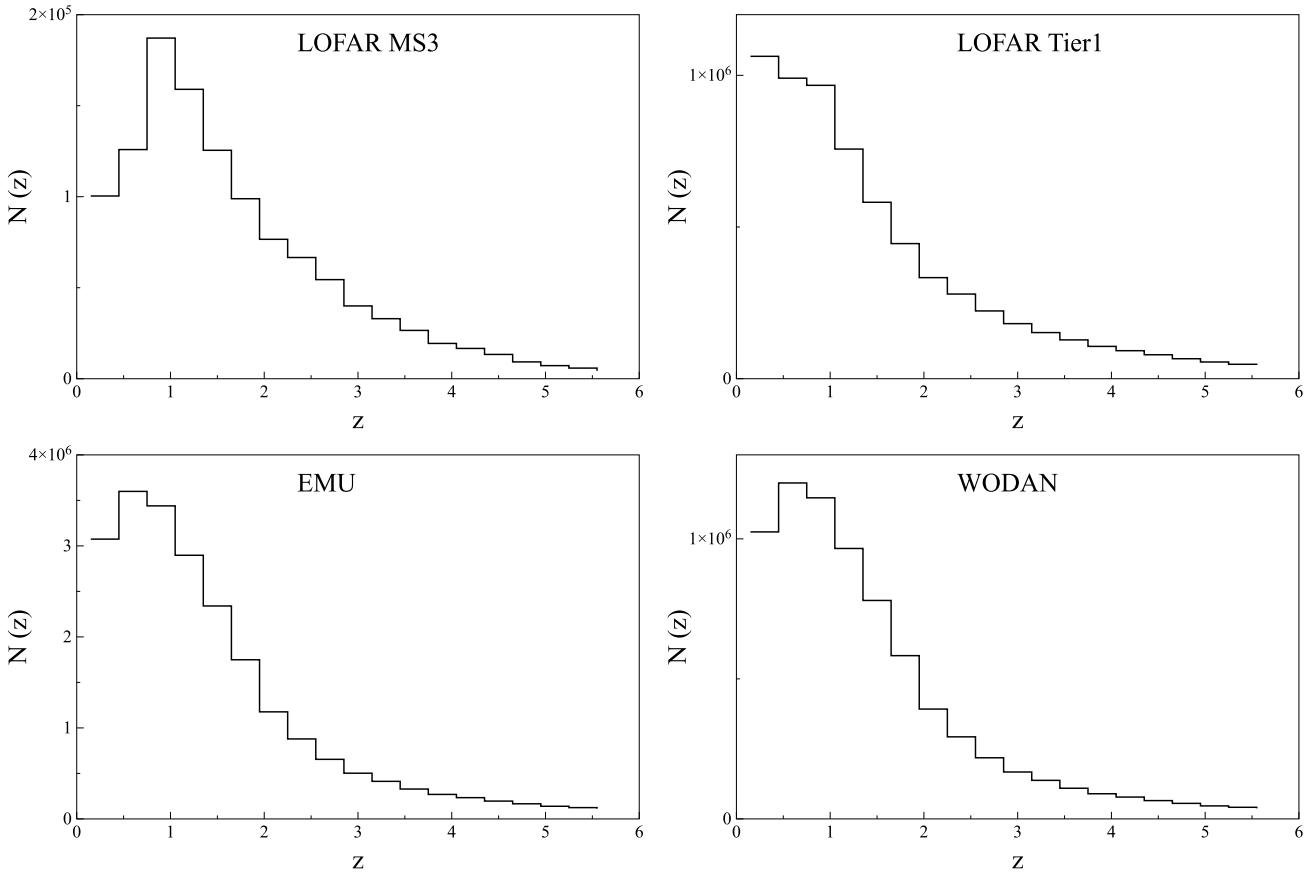


**Figure 1.** Redshift distributions found for the different radio surveys: LOFAR MS$^3$, LOFAR Tier 1, EMU and WODAN. All source types are included in these overall redshift distributions. The vertical axes give the number of sources per bin of width $\Delta z = 0.3$.

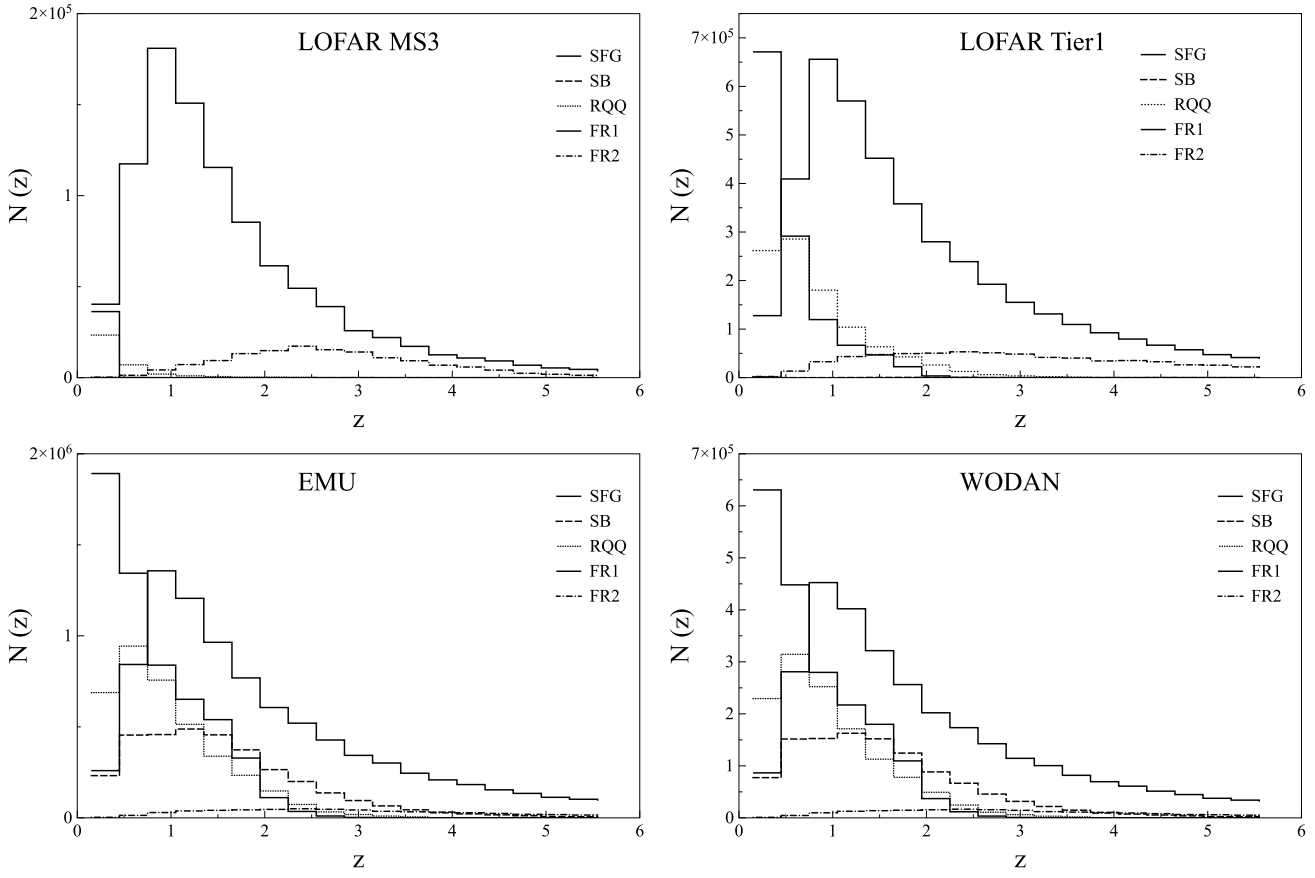


**Figure 2.** Redshift distributions of the LOFAR MS[3], LOFAR Tier 1, EMU and WODAN surveys, for different source types: SFG, star-forming galaxies; SB, starburst; RQQ, radio-quiet quasars; FR I and FR II sources. The vertical axes give the number of sources per bin of width $\Delta z = 0.3$.

by

$$\bar{n}(z, M) = \sqrt{\frac{2qA^2}{\pi}} \frac{3H_0^2\Omega_{0m}}{8\pi G} \frac{\delta_c}{MD(z)\sigma_M} \times \left\{1 + \left[\frac{D(z)\sigma_M}{\sqrt{q}\delta_c}\right]^{2p}\right\} \left|\frac{\mathrm{d}\ln\sigma_M}{\mathrm{d}\ln M}\right| \times \exp\left[-\frac{q\delta_c^2}{2D^2(z)\sigma_M^2}\right]. \quad (2)$$

Here, $\sigma_M^2$ is the mass variance on scale $M$, $\delta_c$ is the critical overdensity for the spherical collapse, $D(z)$ is the linear growth factor of density fluctuations and $q$ and $p$ are parameters to be fitted with simulations (Sheth & Tormen 1999). We can describe the bias by

$$b(M, z) = 1 + \frac{1}{\delta_c}\left[\frac{q\delta_c^2}{D^2(z)\sigma_M^2} - 1\right] + \frac{2p}{\delta_c}\left[\frac{1}{1 + \{\sqrt{q}\delta_c/[D(z)\sigma_M]\}^{2p}}\right]. \quad (3)$$

For the purposes of this paper, we use the bias in the S[3] simulation for each galaxy population, which is computed using the formalism of equations (2) and (3) separately for each galaxy population, where each population is assigned a dark matter halo mass. This dark matter halo mass is chosen to reflect the large-scale clustering found by observations. Note that for most of Fig. 3, there are simply no observational measurements available at present, so large uncertainties in bias remain.

The S[3] simulation provides us with a source catalogue with the sources identified by type (i.e. starburst, FR II radio galaxy, etc.).

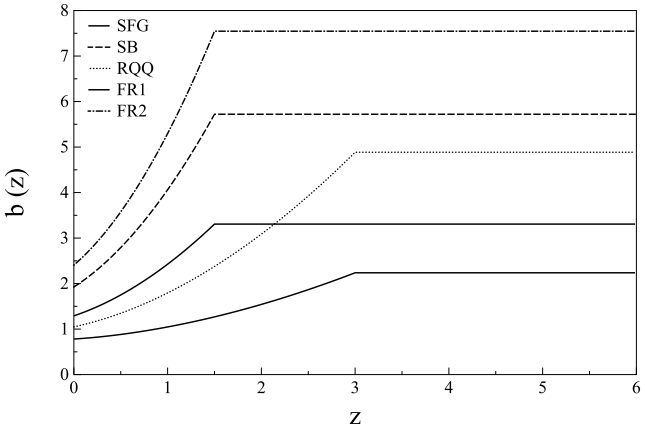


**Figure 3.** Bias as a function of redshift for the different source types, as calculated for our simulated catalogues in accordance with Wilman et al. (2008).

Each of these has a different prescription for the bias, as described in Wilman et al. (2008). With this framework, we find that the increasing bias $b(z)$ with redshift would lead to excessively strong clustering at high redshift. Therefore, the bias for each population is held constant above a certain cut-off redshift, as described by Wilman et al. (2008). Fig. 3 shows the resulting redshift dependence of the bias that we use for the different source types. While this bias evolution is indicative of that expected, the exact behaviour is not yet well known. To allow for this uncertainty, we marginalize over the

overall bias amplitude, and we discuss the remaining uncertainties in Section 8.1.

## 4 COSMOLOGICAL PROBES

In this section, we describe several cosmological probes that can be measured with the forthcoming radio surveys, in combination with surveys at other wavelengths. Here, we describe the necessary framework for calculating the accuracy with which we can measure these probes. We describe the signal-to-noise of the measurements from the specific planned surveys in Section 5.

### 4.1 Autocorrelation function

The first cosmological probe we can examine with the radio surveys is the two-point correlation function of source positions, which is a measure of the degree of clustering in either the spatial, $\xi(r)$, or the angular, $w(\theta)$, distribution of sources. For the current radio surveys, where individual redshifts are unknown, there is little radial information. Therefore, it is appropriate to study only the angular two-point correlation function, $w(\theta)$, which is defined as the excess probability of finding a radio source at an angular distance $\theta$ from another given radio source (Peebles 1980):

$$\delta P = n[1 + w(\theta)]\delta\Omega. \tag{4}$$

Here, $\delta P$ is the probability, $n$ is the mean surface density and $\delta\Omega$ is a surface area element.

The angular two-point correlation function of a given sample of objects can be computed using one of the many estimators that have been proposed (e.g. Hamilton 1993; Landy & Szalay 1993).

Its Fourier transform, the angular power spectrum, can be calculated from the underlying three-dimensional matter power spectrum using

$$C_\ell^{gg} = \left\langle a_{\ell m}^g a_{\ell m}^{g*} \right\rangle = 4\pi \int \frac{\mathrm{d}k}{k} \Delta^2(k) \left[ W_\ell^g(k) \right]^2. \tag{5}$$

Here, $W_\ell^g$ is the radio-source distribution window function described in equation (7), $\Delta^2(k)$ is the logarithmic matter power spectrum at the present time and $a_{\ell m}$ are the spherical harmonics coefficients, assumed to be standard gaussian random variables.

#### 4.1.1 Radio-source window function

Radio-source counts are a biased tracer of the underlying matter distribution. Thus, the projected number density of radio sources per steradian is related to the matter distribution via

$$n(z, \hat{n})\mathrm{d}z\mathrm{d}\Omega = \frac{\mathrm{d}N}{\mathrm{d}z}[1 + b(z)\delta(z, \hat{n})]\,\mathrm{d}z\,\mathrm{d}\Omega. \tag{6}$$

The window function can then be written as (see, for example, Giannantonio et al. 2008a; Raccanelli et al. 2008)

$$W_\ell^g(k) = \int \frac{\mathrm{d}N}{\mathrm{d}z} b(z) D(z) j_\ell[ck\eta(z)]\mathrm{d}z. \tag{7}$$

Here, $(\mathrm{d}N/\mathrm{d}z)\mathrm{d}z$ is the mean number of sources per steradian with redshift $z$ within $\mathrm{d}z$, brighter than the flux limit, $b(z)$ is the bias factor relating the source overdensity to the mass overdensity, assumed to be scale-independent, $D(z)$ is the linear growth factor of mass fluctuations, $j_\ell(x)$ is the spherical Bessel function of order $\ell$ (Bessel 1824) and $\eta(z)$ is the conformal look-back time.

#### 4.1.2 Non-Gaussian clustering

The amplitude and shape of clustering on large scales, described by the Auto-Correlation Function (ACF), can provide important cosmological information. For example, a unique way to test aspects of inflationary theories is to measure the statistics of the initial conditions of cosmological perturbations. An important goal for forthcoming cosmological experiments is to test whether the initial conditions of the probability distribution function of cosmological perturbations deviate from Gaussianity. This can be done using the CMB (Bartolo et al. 2004; Komatsu 2010, and references therein) or the LSS of the Universe (Matarrese, Verde & Jimenez 2000; Dalal et al. 2008; Slosar et al. 2008; Desjacques & Seljak 2010; Xia et al. 2010a). Deviations from Gaussian initial conditions can be parametrized by the dimensionless parameter $f_{\mathrm{NL}}$:

$$\Phi_{\mathrm{NG}} = \phi + f_{\mathrm{NL}} \left( \phi^2 - \langle \phi^2 \rangle \right). \tag{8}$$

Here, $\Phi$ denotes the Bardeen gauge-invariant potential, which, on sub-Hubble scales, reduces to the usual Newtonian peculiar gravitational potential, $\phi$ is a Gaussian random field and the second term, when $f_{\mathrm{NL}}$ is not zero, gives the deviation from gaussianity. In this paper, we refer to the so-called 'local type' $f_{\mathrm{NL}}$ and we use the LSS convention (as opposed to the CMB convention, where $f_{\mathrm{NL}}^{\mathrm{LSS}} \sim 1.3 f_{\mathrm{NL}}^{\mathrm{CMB}}$; Xia et al. 2010a).

One method for constraining non-Gaussianity from LSS surveys exploits the fact that a positive $f_{\mathrm{NL}}$ corresponds to positive skewness of the density probability distribution, and hence an increased number of massive objects (Matarrese et al. 2000; Dalal et al. 2008; Desjacques & Seljak 2010).

In particular, a non-zero $f_{\mathrm{NL}}$ in equation (8) introduces a scale-dependent modification of the large-scale halo bias, so that the difference from the usual Gaussian bias is

$$\Delta b(z, k) = [b_{\mathrm{G}}(z) - 1] f_{\mathrm{NL}} \delta_{\mathrm{ec}} \frac{3\Omega_{0m} H_0^2}{c^2 k^2 T(k) D(z)}. \tag{9}$$

Here, $b_{\mathrm{G}}(z)$ is the usual bias that is calculated by assuming Gaussian initial conditions, which are assumed to be scale-independent, $D(z)$ is the linear growth factor and $\delta_{\mathrm{ec}}$ is the critical value of the matter overdensity for ellipsoidal collapse, $\delta_{\mathrm{ec}} = \delta_{\mathrm{c}}\sqrt{q}$.

### 4.2 Integrated Sachs–Wolfe effect

In addition to making an autocorrelation of source positions, it is possible to cross-correlate the radio-source distribution with CMB temperature maps, in order to detect the ISW effect (Sachs & Wolfe 1967). Travelling from the last scattering surface to us, CMB photons pass through gravitational potential wells of intervening matter. In an Einstein–de Sitter universe, the blueshift of a photon falling into a well is cancelled by the redshift as it climbs out. However, in a universe with a dark energy component or modification to GR, the local gravitational potential $\Phi$ varies with time, so potential wells are stretched while photons are traversing the well. This leads to a net blueshift of the photons, and equivalently to a net change in photon temperature, which accumulates along the photon path and is proportional to the time variation of the gravitational potential.

The ISW effect only contributes to the low $\ell$ multipoles of the CMB fluctuations, and it is smaller than the primary CMB anisotropies even at those $\ell$. Thus, to make the effect detectable, we have to cross-correlate CMB maps with tracers of large-scale structure (Crittenden & Turok 1996; Boughn & Crittenden 2012; Boughn & Crittenden 2004), such as radio sources, because the source density traces the potential wells. If the evolution of potentials is modified by dark energy, we should observe a correlation

between CMB temperature anisotropies and the source distribution. For this reason, ISW measurements will provide a signature for dark energy or modified gravity. The *Wilkinson Microwave Anisotropy Probe* (*WMAP*) data have been cross-correlated with a variety of radio, infrared, optical and X-ray surveys (e.g. Giannantonio et al. 2006, 2008a; Pietrobon, Balbi & Marinucci 2006; Raccanelli et al. 2008; Ho et al. 2008; see Dupe et al. 2010 for a review of recent results and more references) to look for evidence of a decay of the gravitational potential as a result of the influence of dark energy.

We can write the cross-correlation power spectrum between the surface density fluctuations of radio sources and CMB temperature fluctuations as

$$C_\ell^{gT} = \left\langle a_{\ell m}^g a_{\ell m}^{T*} \right\rangle = 4\pi \int \frac{\mathrm{d}k}{k} \Delta^2(k) W_\ell^g(k) W_\ell^T(k), \tag{10}$$

where $W_\ell^g$ and $W_\ell^T$ are the radio source and CMB window functions, respectively, and $\Delta^2(k)$ is the logarithmic matter power spectrum at the present time.

The cross-correlation function as a function of the angular separation $\theta$ is then obtained as

$$C^{gT}(\theta) = \sum_\ell \frac{2\ell+1}{4\pi} C_\ell^{gT} L_\ell(\cos\theta), \tag{11}$$

where $L_\ell$ are the Legendre polynomials of order $\ell$ (Legendre 1785).

#### *4.2.1 Integrated Sachs–Wolfe window function*

In the Newtonian gauge, scalar metric perturbations are specified by the gauge-invariant potentials $\Psi$ and $\Phi$:

$$\mathrm{d}s^2 = -a^2(\tau)[(1+2\Psi)\mathrm{d}\tau^2 - (1-2\Phi)\mathrm{d}\boldsymbol{x}^2]. \tag{12}$$

The temperature anisotropies resulting from the ISW effect are expressed by an integral over the conformal look-back time from the present time ($\eta = 0$) to the CMB decoupling surface $\eta_{\mathrm{dec}}$:

$$\Theta_{\mathrm{ISW}} = \frac{\delta T}{T} = -\frac{1}{c^2} \int_0^{\eta_{\mathrm{dec}}} (\dot{\Phi} + \dot{\Psi})\, \mathrm{d}\eta. \tag{13}$$

Here, $\tau$ is the conformal time, the dot represents a conformal time derivative and the integral is calculated along the line of sight of the photon. In the absence of anisotropic stress, the momentum constraint in GR fixes $\Phi = -\Psi$. So, the ISW modification of the temperature of the CMB in GR becomes

$$\Theta_{\mathrm{ISW}} = \frac{\delta T}{T} = -\frac{2}{c^2} \int_0^{\eta_{\mathrm{dec}}} \frac{\partial \Phi}{\partial \eta}\, \mathrm{d}\eta. \tag{14}$$

The local gravitational potential is related to the matter distribution via the Poisson equation

$$\nabla^2 \Phi = 4\pi G a^2 \varrho_m \delta_m, \tag{15}$$

where the gradient is taken with respect to comoving coordinates. Taking the Fourier transform, we have

$$\Phi(k,\eta) = -\frac{3}{2}\Omega_{0\mathrm{m}} \left(\frac{H_0}{ck}\right)^2 g(\eta)\delta(k), \tag{16}$$

where $H_0$ is the Hubble constant, $g(\eta) \equiv D(\eta)/a(\eta)$ is the linear growth suppression factor and $\delta(k)$ is the mass overdensity field.

Combining equations (15) and (16), the window function for the ISW effect can be written as

$$W_\ell^T(k) = 3\Omega_{0\mathrm{m}} \left(\frac{H_0}{ck}\right)^2 \int \frac{\partial \Phi}{\partial z} j_\ell[ck\eta(z)]\, \mathrm{d}z, \tag{17}$$

where $\Phi(z)$ is the Newtonian gravitational potential.

### 4.3 Magnification bias

Light rays are deflected by large-scale structures along the line of sight, which therefore systematically introduce distortions in the observed images of distant sources. This is the phenomenon of gravitational lensing. The sources behind a lens are magnified in size, while surface brightness is conserved. This leads to an increase in the total observed luminosity of a source.

Observationally, we can detect the effects of magnification by cross-correlating two galaxy surveys with disjoint redshift distributions. In this paper, we consider the possibility of using an optical survey, such as the Sloan Digital Sky Survey II (SDSS-II; Abazajian et al. 2009) or the DES,[5] for our low-redshift 'lens' sample – Pan-STARRS will also be available on these time-scales and could also be used. This will serve as the foreground that magnifies the background radio distribution. We discuss this further in Section 5.3.

This 'cosmic magnification' effect was first detected by Scranton et al. (2005), who cross-correlated foreground SDSS galaxies with SDSS quasars. More recently, Hildebrandt, van Waerbeke & Erben (2009) have detected the effect in samples of normal galaxies in the Canada–France–Hawaii Telescope Legacy Survey (CFHTLS), Wang et al. (2011) have detected the effect at longer wavelengths using *Herschel*, while Ménard et al. (2010) have built on the SDSS analysis by constraining galaxy–mass and galaxy–dust correlation functions.

The effect can be described in detail as follows. At position $\varphi$, we can relate the behaviour of unlensed sources with number density $N_0(m)\,\mathrm{d}m$ within a magnitude range $[m, m + \mathrm{d}m]$, to that of lensed sources with number density $N(m, \varphi)\,\mathrm{d}m$. There are two competing effects in this relationship: the flux increase as a result of magnification of distant faint sources, which increases the number density of observed images above a certain magnitude threshold, and, counteracting this, the dilution of the number density as a result of the stretching of the solid angle by lensing. If the source fluxes have a distribution with a power-law slope given by

$$\alpha(m) = 2.5 \frac{\partial[\log N_0(m)]}{\partial m}, \tag{18}$$

we can obtain (Bartelmann & Schneider 2001)

$$N(m,\varphi)\,\mathrm{d}m = \mu^{\alpha(m)-1} N_0(m)\,\mathrm{d}m. \tag{19}$$

Here, the magnification $\mu$ is

$$\mu = \frac{1}{|(1-\kappa)^2 - |\gamma|^2|}, \tag{20}$$

where the convergence $\kappa$ and the shear $\gamma$ are two further lensing distortions. In the weak lensing regime, it is possible to Taylor expand the last equality in equation (20) to obtain

$$\mu(\varphi) \simeq 1 + 2\kappa(\varphi). \tag{21}$$

Therefore, we see that the magnification is closely related to the convergence $\kappa$, which is related to the matter overdensity via a line-of-sight integral (Bartelmann & Schneider 2001):

$$\kappa(\varphi) = \frac{3\Omega_{0\mathrm{m}} H_0^2}{2c^2} \int_0^{w_{\mathrm{H}}} \mathrm{d}w\, W(w) f_{\mathrm{K}}(w) \frac{\delta[f_{\mathrm{K}}(w)\varphi, w]}{a(w)}. \tag{22}$$

Here, $\varphi$ is the angular position on the sky, $w_{\mathrm{H}}$ is the horizon distance, $w(z)$ is the comoving radial distance, $f_{\mathrm{K}}(w)$ is the angular diameter

[5] http://www.darkenergysurvey.org/

comoving distance, $a$ is the scalefactor and a quantity $W$ involves the redshift distribution and geometry

$$W(w) = \int_{w}^{w_{\rm H}} {\rm d}w' Z_w(w') \frac{f_{\rm K}(w'-w)}{f_{\rm K}(w')}, \quad (23)$$

where $Z_w(w)\,{\rm d}w$ is the source redshift distribution.

Because of the magnification bias effect described, we can obtain cosmological constraints by cross-correlating foreground and background objects. Hence, we can investigate how clustered lensed background sources appear to be around foreground sources, compared to a random distribution. The most common estimator of the angular two-point correlation (also adopted in this work) is given by

$$\xi_{\rm SL} = [\bar{N}_{\rm S}\bar{N}_{\rm L}]^{-1}\overline{[N_{\rm S}(\varphi) - \bar{N}_{\rm S}][N_{\rm L}(\varphi+\phi) - \bar{N}_{\rm L}]}, \quad (24)$$

where, in our case, the 'S' and 'L' indices denote background sources and foreground lenses, respectively, and overbarred quantities correspond to averaged quantities.

Large-scale structures only slightly magnify or demagnify sources, so we can write

$$\mu^{\alpha-1} = (1+\delta\mu)^{\alpha-1} \simeq 1 + (\alpha-1)\delta\mu, \quad (25)$$

leading to an over/underdensity in background sources:

$$\frac{N_{\rm S}(\varphi) - \bar{N}_{\rm S}}{\bar{N}_{\rm S}} \simeq (\alpha-1)\delta\mu(\varphi). \quad (26)$$

Assuming that foreground sources have bias $b_{\rm L}$, the number density can be related to the underlying matter density contrast by

$$\frac{N_{\rm L} - \bar{N}_{\rm L}}{\bar{N}_{\rm L}} = b_{\rm L}\delta(\varphi). \quad (27)$$

Then, as a consequence (cf. Bartelmann & Schneider 2001), $\xi_{\rm SL}(\varphi)$ is related to the theoretical magnification density contrast two-point correlation function $\xi_{\mu\delta}(\varphi)$ via

$$\xi_{\rm SL}(\varphi) = (\alpha-1)b_{\rm L}(\varphi)\xi_{\mu\delta}(\varphi), \quad (28)$$

with

$$\xi_{\mu\delta}(\varphi) = \frac{3H_0^2\Omega_0}{2\pi c^2}\int {\rm d}w \frac{W(w)G_{\rm f}(w)}{a(w)f_{\rm K}^2(w)}\int k\,{\rm d}k P_\delta(k) J_0(k\varphi). \quad (29)$$

Here, $P_\delta(k)$ is the matter power spectrum, $G_{\rm f}(w)$ is the foreground redshift distribution and $W(w)$ is the source lensing efficiency distribution given in equation (23).

It is only when $\alpha \neq 1$ that we obtain magnification bias. We obtain a positive cross-correlation only when $\alpha > 1$, and anticorrelation when $\alpha < 1$. Equations (28) and (29) show how magnification bias observations allow us to measure information about the amplitude, shape and evolution of the matter power spectrum, together with information about the bias and geometrical factors in the expanding background.

From equation (29), we can also obtain the cosmic magnification power spectrum (Bartelmann & Schneider 2001):

$$C_\ell^{g\mu} = \left\langle a_{\ell m}^g a_{\ell m}^{\mu *}\right\rangle = \int \frac{{\rm d}k}{k}\Delta^2(k) W_\ell^g(k) W_\ell^\mu(k). \quad (30)$$

Here, $W_\ell^g(k)$ has the same meaning as in equation (5) and $W_\ell^\mu(k)$ contains the pre-factors and $w$ integral from equations (28) and (29).

## 5 PREDICTIONS FOR MEASUREMENTS WITH FORTHCOMING SURVEYS

### 5.1 Autocorrelation predictions

We computed the predicted autocorrelation source power spectra for LOFAR, EMU and WODAN using equation (5). The errors were assumed to follow

$$\sigma_{C_\ell^{gg}} = \sqrt{\frac{2\left[C_\ell^{gg} + (1/\bar{n})\right]^2}{(2\ell+1)f_{\rm sky}}}, \quad (31)$$

where $f_{\rm sky}$ is the sky coverage of the survey and $\bar{n}$ is the mean number of sources per steradian. This assumes that systematics are subdominant, and there are no effects from the finite size of objects (i.e. we are not close to the confusion limit).

Fig. 4 shows $C_\ell^{gg}$ for the combined source populations of the four different surveys considered. As shown, the errors on large and small scales are more pronounced because they are dominated by cosmic variance and shot noise, respectively. At intermediate scales, surveys with a higher number density will provide the best measurements (in this case, EMU). We examine what can be learned cosmologically from these measurements in Section 7.

Fig. 5 plots the predicted source power spectrum of EMU radio sources for different values of the non-Gaussianity parameter $f_{\rm NL}$. The black solid line is the standard Gaussian prediction, the other lines are the predictions for non-Gaussian clustering and the shaded area is $1\sigma$ errors (per mode) as in equation (31). The presence of the non-Gaussian bias of equation (9) enhances the clustering at large scales, thus increasing the amplitude of the autocorrelation function at those scales. A $\chi^2$ analysis shows that EMU should be able to distinguish (at the $1\sigma$ level) a $f_{\rm NL}$ of 8 from a purely Gaussian model. It is worth noting that the current limit on $f_{\rm NL}$ from *WMAP* 7-yr data is $f_{\rm NL}^{\rm LSS} = 42 \pm 27$ at 68 per cent confidence level (Komatsu et al. 2011),[6] and any detection of $f_{\rm NL} > 1$ would rule out all single scalar field inflation models (Komatsu 2010).

It is intriguing to note that the observed autocorrelation function of the NVSS has a shape that differs from the ΛCDM prediction at relatively large angular separation (Xia et al. 2010a). The observed behaviour can be explained using a non-Gaussian correction (Xia et al. 2010a), a peculiar bias model (Raccanelli et al. 2008) or some systematic errors not yet found in the NVSS. The degeneracy between models of bias and non-Gaussian corrections can be broken because their effect has a different redshift and scale dependence (the non-Gaussian correction is important only at large scales, because of the $1/k^2$ term in equation 9).

It is also interesting to note that a similar excess power at large scales has been found in spectroscopic (Kazin et al. 2010; Samushia, Percival & Raccanelli 2012) and photometric (Thomas, Abdalla & Lahav 2011) data sets, although Ross et al. (2011) have suggested that this is likely to be a result of masking effects from stellar sources. With the forthcoming all-sky radio surveys, measuring the angular autocorrelation will be an interesting check for this problem. However, the CMB shows a lack of correlation at angular scales >60 deg (Copi et al. 2010; Bennett et al. 2011), which is discrepant with the concordance model of cosmology. The significance and origin of this are unclear. Certainly, radio surveys that cover large fractions of the full sky will help to resolve this puzzle.

[6] Note that in the CMB convention this is $32 \pm 21$.

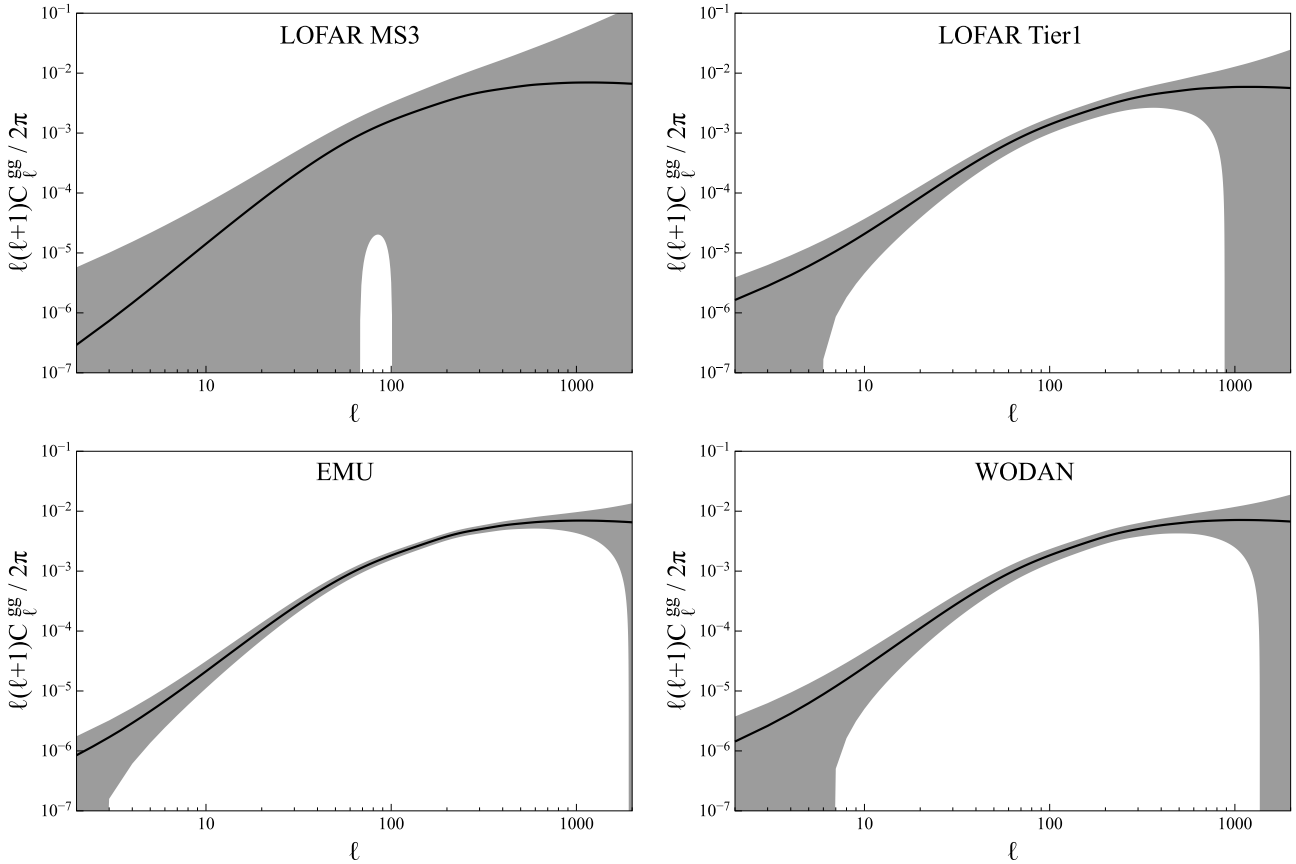


**Figure 4.** Source power spectra (equation 5) of the combined source populations (black solid lines) for the different surveys, with $1\sigma$ errors (grey shaded regions), as in equation (32).

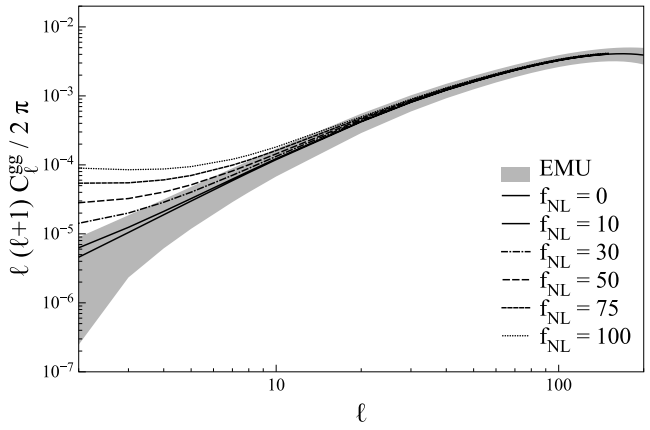


**Figure 5.** Source power spectrum of EMU radio sources for different values of the non-Gaussianity parameter $f_{\rm NL}$. The shaded regions are errors for the EMU survey, as in equation (31).

### 5.2 Cross-correlation predictions

As we have seen in Section 4.2, the cross-correlation between the CMB and the LSS depends on various factors from both of the window functions in equation (10). It is influenced by the evolution of the gravitational potential (equation 17) and by the clustering and bias of structures (equation 7). For this reason, it has been used to test and constrain cosmological issues, such as the evolution and clustering of structures (Raccanelli et al. 2008; Schaefer, Douspis & Aghanim 2009; Massardi et al. 2010), models of dark energy (Pogosian et al. 2005; Xia et al. 2009) and alternative models for the gravitational potential, such as the Dvali-Gabadadze-Porrati (DGP), unified dark matter (UDM) cosmologies and Brans–Dicke theories (Giannantonio, Song & Koyama 2008b; Bertacca et al. 2011; De Felice et al., in preparation).

The detection of the ISW effect via the cross-correlation of the LSS with the CMB is cosmic-variance limited, as it affects only the largest angular scales. Therefore, the best measurement possible is a complete full-sky survey with negligible shot noise. Regarding the CMB, the data provided by *WMAP* are already precise enough at low $\ell$, and the improvement that *Planck* will provide does not substantially affect the ISW detection significance.

Fig. 6 shows the predicted cross-correlations of the CMB with the combined radio-source distributions. The solid lines are the standard $\Lambda$CDM+GR model and the shaded regions are the errors, calculated using (e.g. Cabre et al. 2007)

$$\sigma_{C_\ell^{gT}} = \sqrt{\frac{\left(C_\ell^{gT}\right)^2 + C_\ell^{gg} C_\ell^{TT}}{(2\ell+1) f_{\rm sky}}}, \tag{32}$$

where $f_{\rm sky}$ is the sky coverage of the survey. The shot noise should be negligible for the cross-correlation of the CMB with LOFAR Tier1, EMU and WODAN on the scales of interest, given the high number density per $\ell$ mode.

Fig. 7 shows the predicted cross-correlation function, with cosmic variance errors, for the WODAN survey (light grey area), the WODAN+EMU combination (dark grey area) and the measured

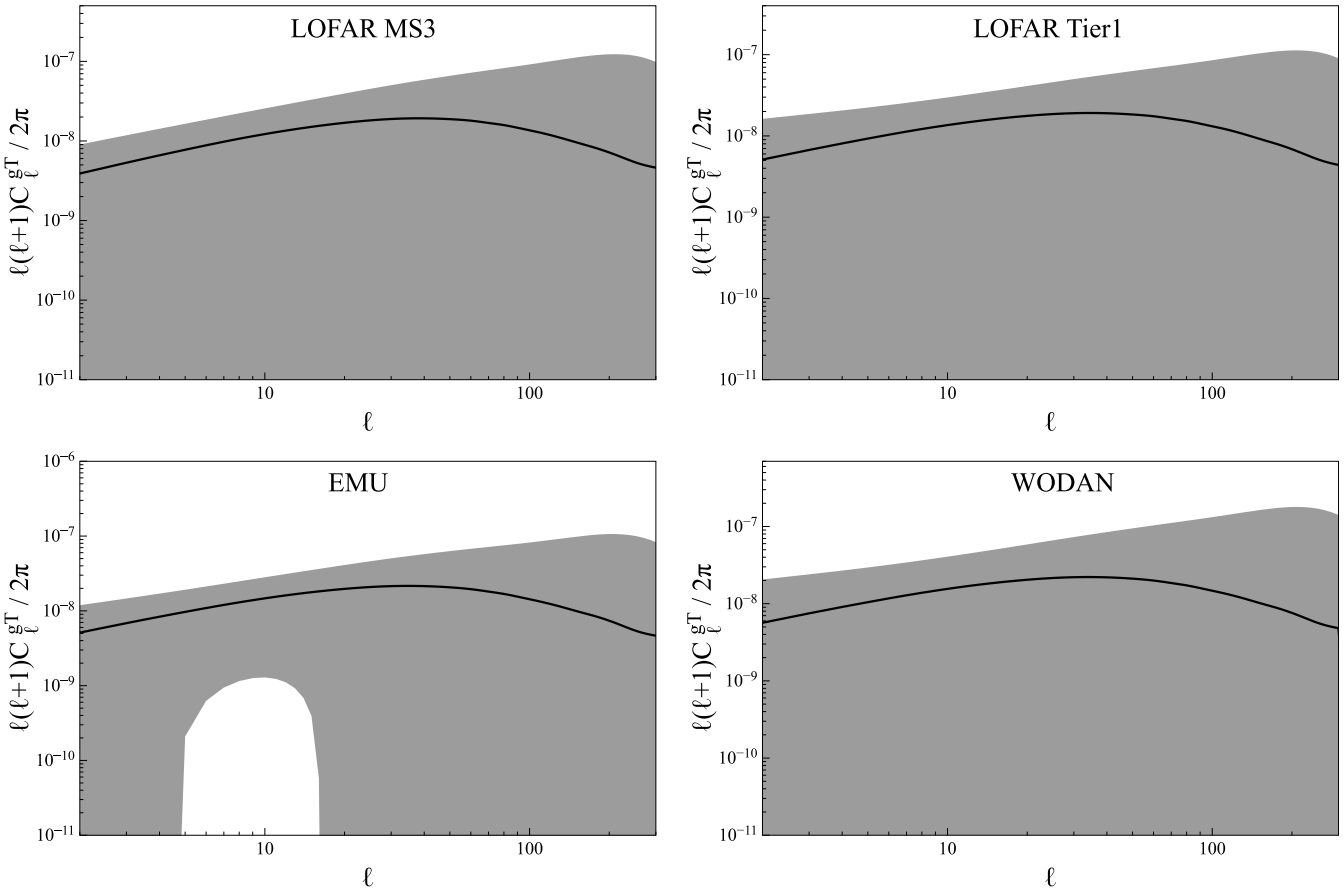


**Figure 6.** Cross-correlations of radio sources with the CMB (equation 11). The solid lines are the theoretical ΛCDM prediction, and the shaded area corresponds to cosmic variance errors per mode, as in equation (32).

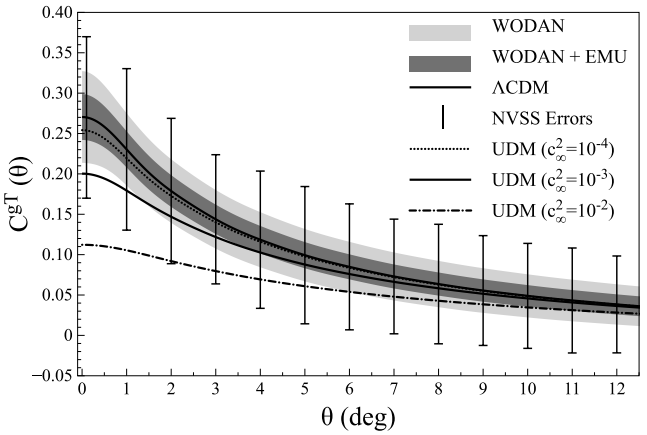


**Figure 7.** Cross-correlation of WODAN sources with the CMB. The black solid line is the ΛCDM prediction and the black dashed line is the UDM prediction for $c_\infty^2 = 10^{-2}$ (see text for details). The shaded regions are errors, with light grey for the WODAN survey and dark grey for the EMU+WODAN combination, and the error bars are the NVSS errors.

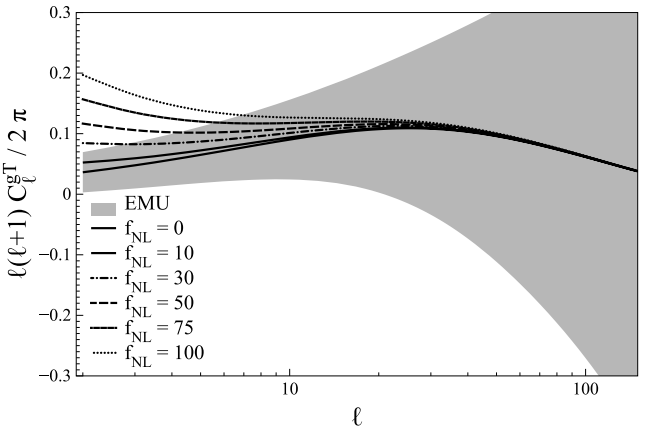


**Figure 8.** Cross-power spectrum of EMU radio sources with the CMB (equation 10) for different values of the non-Gaussianity parameter $f_{NL}$. The shaded regions are errors for the EMU survey, as in equation (32).

NVSS errors (error bars) as a comparison. Note the substantial improvement in the ISW measurements provided by the all-sky survey, compared to NVSS or WODAN alone.

The enhanced clustering resulting from non-Gaussianity would also modify the cross-correlation of galaxies with the CMB (Xia et al. 2010b), through the modified bias of equation (9) in the galaxy window function (equation 7). The effect is more significant on the largest scales, as shown in Fig. 8, which presents the cross-correlation of the CMB with EMU radio sources for different values of $f_{NL}$. As in the autocorrelation case, we performed a $\chi^2$ analysis to predict what level of non-Gaussianity we should be able to detect. Again, we used the simulations of EMU data because its ISW detection should be the best of the surveys analysed (see Fig. 6). We found that these data would detect a $f_{NL}$ of 11 at the $1\sigma$ level.

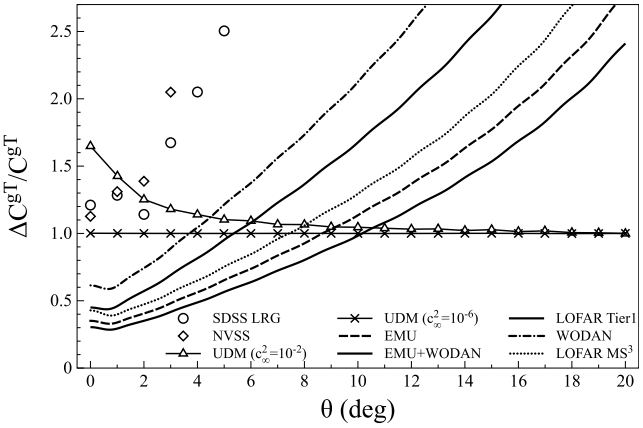


**Figure 9.** Constraining power of cross-correlation CMB–radio sources for the different surveys. The lines are radio surveys used in this paper, and the symbols are measurements from NVSS and SDSS. The lines connecting the symbols are thresholds to detect UDM models with a non-zero speed of sound (see text for details).

As an initial example of cosmological constraints, in Fig. 7, the black dashed line is the predicted cross-correlation function for UDM scalar field cosmologies, where dark matter and dark energy are part of a single component. The key parameter in this model is the speed of sound (at the present time) of the dark component, $c_\infty^2$, which should be different from zero but small enough to allow the dark component to cluster (for details, see Bertacca et al. 2008, 2011). The detection of a non-zero speed of sound would be an indication of a non-ΛCDM universe.

Using NVSS, we are able to see differences from the ΛCDM case from $c_\infty^2 = 10^{-2}$, while the plot in Fig. 7 shows that by using the combined full-sky EMU+WODAN we can constrain values of the speed of sound of $c_\infty^2 = 10^{-4}$, using the ISW effect. Further details and forecasts on how well we are able to test UDM cosmological models with these surveys will be part of a subsequent paper.

To predict the significance and constraining power of ISW measurements with the forthcoming radio surveys, in Fig. 9 we define $\Delta C^{gT}/C^{gT}$ as the width of the entire $1\sigma$ constraint, that is

$$\frac{\Delta C^{gT}}{C^{gT}} = \frac{[C^{gT}(\theta) + \sigma_{C^{gT}}] - [C^{gT}(\theta) - \sigma_{C^{gT}}]}{C^{gT}(\theta)} = \frac{2\sigma_{C^{gT}}}{C^{gT}}, \qquad (33)$$

where $\sigma_{C^{gT}}$ is the error on the cross-correlation function in real space. Fig. 9 shows $\Delta C^{gT}/C^{gT}$ (equation 33) for the total surveys. We compare these with current measurements of $\Delta C^{gT}/C^{gT}$ from cross-correlations of NVSS and SDSS LRGs with *WMAP* maps, along with the threshold to actually distinguish between ΛCDM and other cosmological models.

As we can see, for small values of $\theta$, the constraining power is maximum, and all the surveys considered should have an increased discriminatory power. In the case of whole-sky combined surveys, we find that $\Delta C^{gT}/C^{gT}$ is less than half of that of NVSS and SDSS, for small $\theta$.

### 5.3 Magnification bias

We compute the power spectra for the magnification bias using equation (30). We consider the experiment where background radio sources from LOFAR, EMU and WODAN are cross-correlated with foreground galaxies from SDSS for the Northern hemisphere and DES for the Southern hemisphere. We expect to have much better and wider data than the SDSS on the time-scale of the radio surveys considered with the Pan-STARRS $3\pi$ sr survey (Kaiser et al. 2010). When complete, this survey will provide imaging data to a depth between SDSS and DES, so our analysis should be considered as conservative. In the Northern sky, we use SDSS galaxies up to $z = 0.35$ and radio sources as the background for higher redshift, while for the Southern sky we use DES foregrounds up to $z = 1$ and EMU sources as a background. To avoid the overlap between foreground and background galaxies, we remove the LOFAR, EMU and WODAN galaxies at $z < 1$ (i.e. we assume that by cross-matching between optical and radio bands, low-$z$ radio sources can be removed from our sample). We assume that the bias for the foreground galaxies is unity because they are located at low redshifts. We follow Scranton et al. (2005) in measuring the weighted average power-law slope $\langle\alpha - 1\rangle$, where $\alpha$ is given by equation (18). From our simulations, we obtain $-0.219$, $-0.147$, 0.1027 and 0.121 for LOFAR MS$^3$, LOFAR Tier 1, EMU and WODAN, respectively.

Fig. 10 shows the cross-correlation of radio background with the optical power spectra of foreground sources, computing the errors according to Zhang & Pen (2006):

$$\sigma_{C_\ell^{g\mu}} = \sqrt{\frac{C_{\mu g}^2 + \left(C_g^{\rm b} + C_{\rm shot}^{\rm b}\right)\left(C_g^{\rm f} + C_{\rm shot}^{\rm f}\right)}{(2\ell+1) f_{\rm sky}}}. \qquad (34)$$

Here, the superscripts 'f' and 'b' denote the foreground and background sources, respectively, and 'shot' denotes the shot noise.

We can see that by using this probe we have better constraining power when we have a higher number density and magnification index. The EMU will provide moderate constraints for this probe in combination with the DES. We emphasize that a limiting factor for the Northern surveys (LOFAR and WODAN) in our analysis is actually the optical data. We would be able to tighten constraints for these surveys if Pan-STARRS data were used as a foreground instead of SDSS data.

## 6 COSMOLOGICAL MODEL CONSTRAINTS

Having calculated the constraints on each cosmological probe, it is now possible to determine how the LOFAR, EMU and WODAN surveys can improve the measurements of cosmological parameters.

Starting from the Einstein field equation,

$$G_{\mu\nu} = \frac{8\pi G}{c^4} T_{\mu\nu}, \qquad (35)$$

where $G_{\mu\nu}$ is the Einstein tensor, $T_{\mu\nu}$ is the energy-momentum tensor and $G$ is the Newton gravitational constant, we study the improvements that these surveys will bring to the measurement of parameters in the dynamical dark energy and modified gravity scenarios. We investigate these issues using Fisher matrix techniques, following Zhao et al. (2009).

### 6.1 Dynamical dark energy

In the cosmological framework of GR, it has been necessary to modify equation (35) to account for the observed acceleration of the expansion of the Universe. The simplest modification is the introduction of a cosmological constant, as first suggested by Zel'dovich (1967), which can be interpreted as vacuum energy. In this case, the right-hand side of equation (35) is modified:

$$G_{\mu\nu} = T_{\mu\nu} + T_{\mu\nu}^{\rm vac}. \qquad (36)$$

Throughout this section, we set $G = 1/8\pi$ and $c = 1$ for simplicity, and

$$T_{\mu\nu}^{\rm vac} = -\Lambda g_{\mu\nu}. \qquad (37)$$

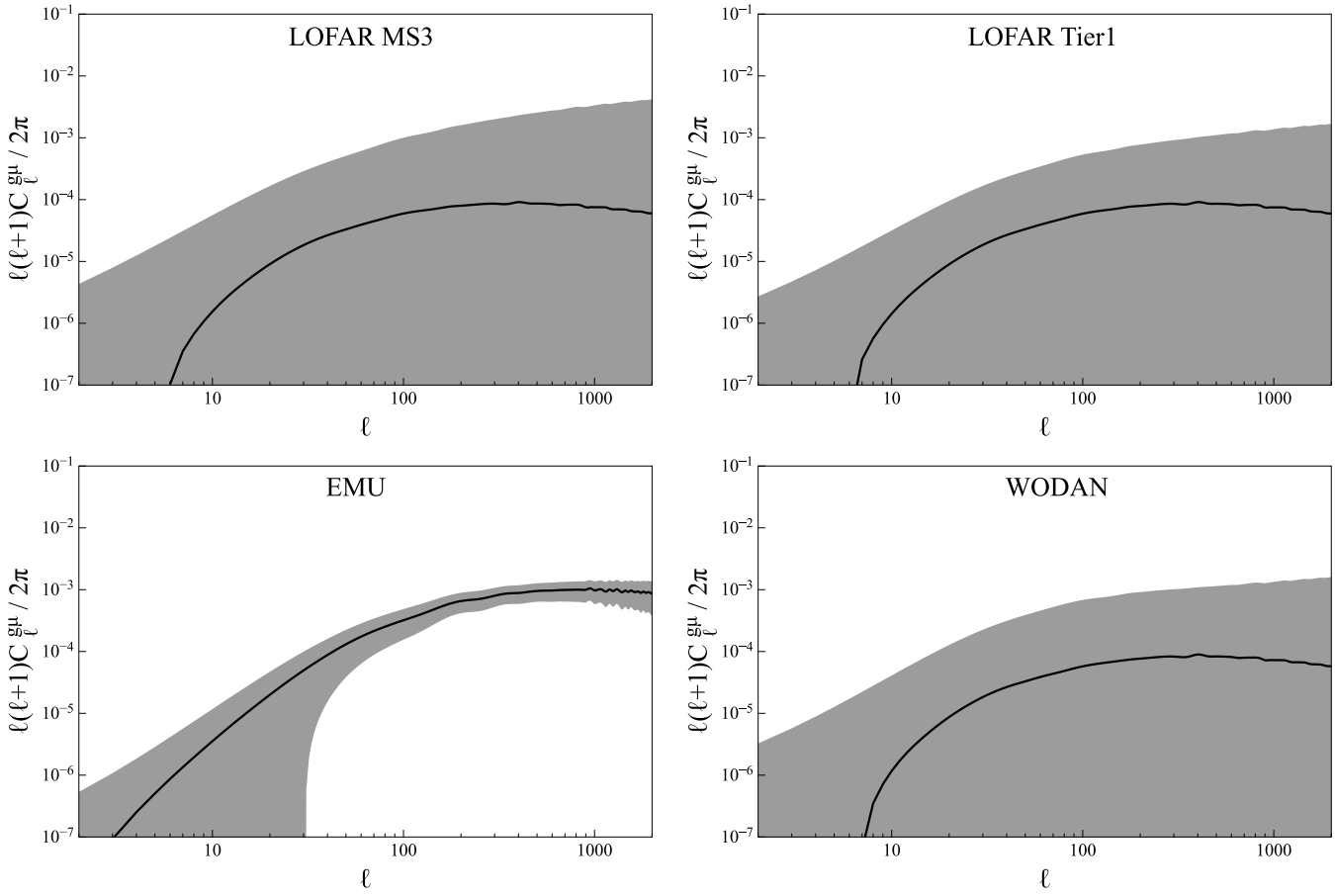


**Figure 10.** Magnification power spectra for LOFAR–SDSS, EMU–DES and WODAN–SDSS. The black solid lines are theoretical predictions (equation 30) and the shaded regions are errors, as in equation (34).

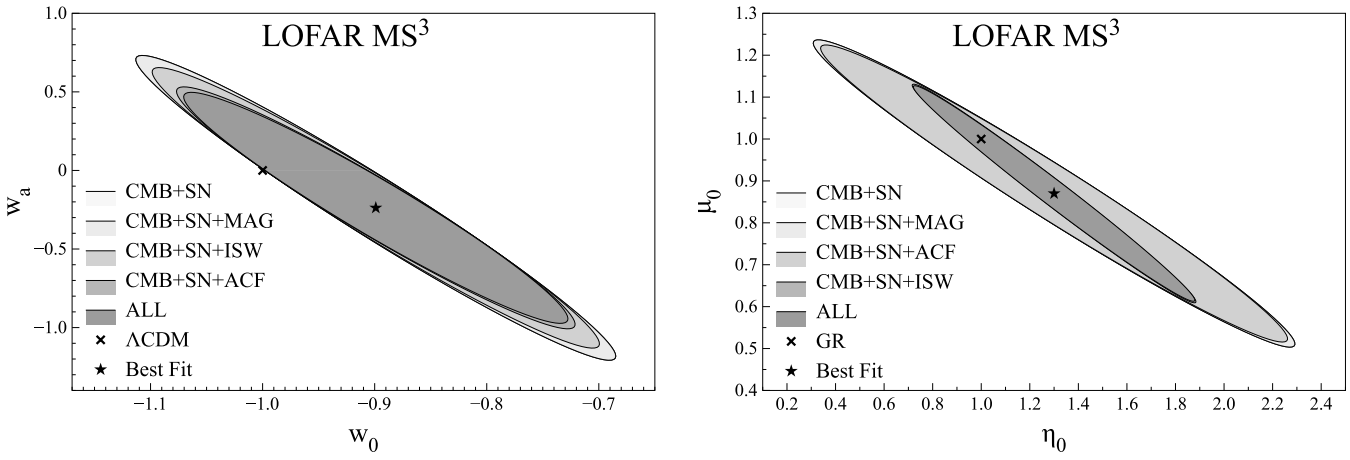


**Figure 11.** Forecast of constraints for the dark energy (left) and modified gravity (right) parameters, for the LOFAR MS$^3$ survey. Ellipses show $1\sigma$ constraints for different combinations of probes (see text for details). Some probes give very similar errors, so all five ellipses are not always visible.

The first step towards understanding the nature of dark energy is to clarify whether it is a simple cosmological constant or whether it originates from other sources that dynamically change in time. The dynamical models can be distinguished from the cosmological constant by considering the evolution of the equation of state of dark energy

$$w = \frac{p}{\varrho}, \tag{38}$$

where $p$ and $\varrho$ are the pressure density and energy density of the fluid, respectively. In the cosmological constant model, $w = -1$, while for dynamical models $w = w(a)$.

To evaluate the potential of the radio surveys considered to constrain the dynamics of different models of dark energy, we adopt the following parametrization for the dark energy equation of state $w$ (Linder 2003):

$$w(a) = w_0 + w_a(1 - a). \tag{39}$$

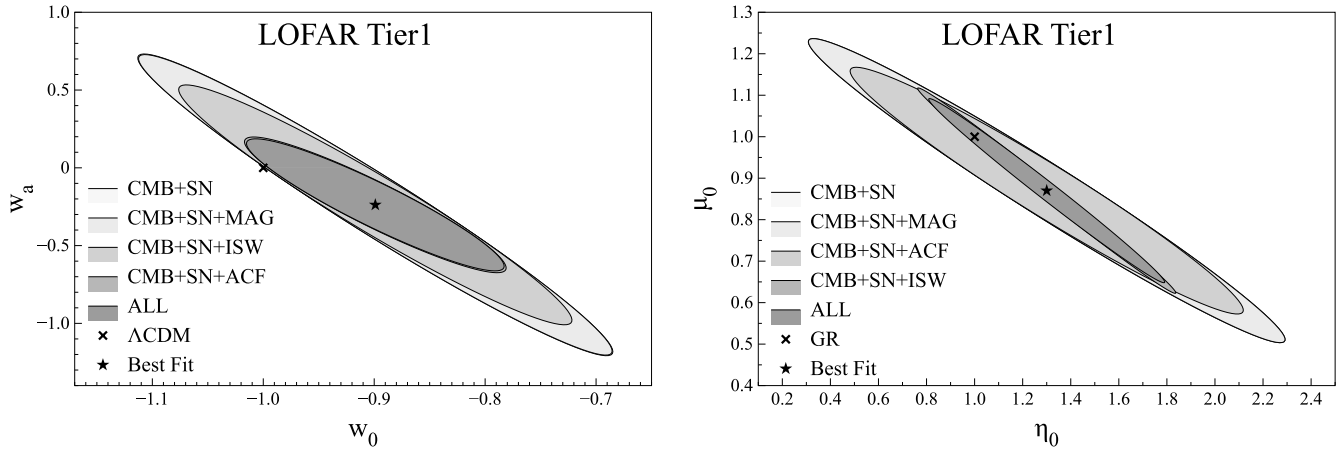


**Figure 12.** Forecast of constraints for the dark energy (left) and modified gravity (right) parameters, for the LOFAR Tier 1 survey. Ellipses show $1\sigma$ constraints for different combinations of probes (see text for details). Some probes give very similar errors, so all five ellipses are not always visible.

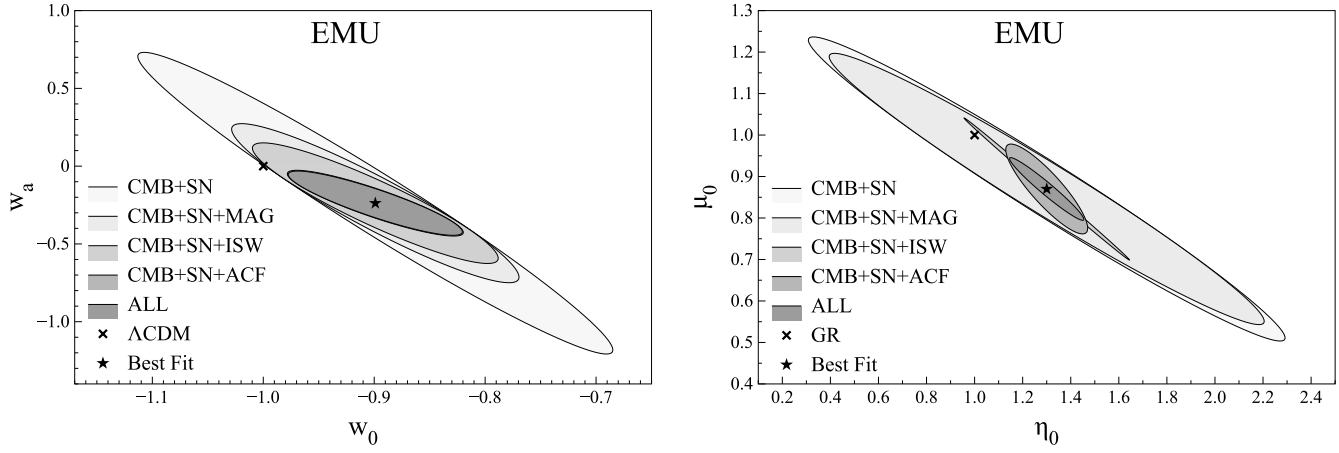


**Figure 13.** Forecast of constraints for the dark energy (left) and modified gravity (right) parameters, for the EMU survey. Ellipses show $1\sigma$ constraints for different combinations of probes (see text for details). Some probes give very similar errors, so all five ellipses are not always visible.

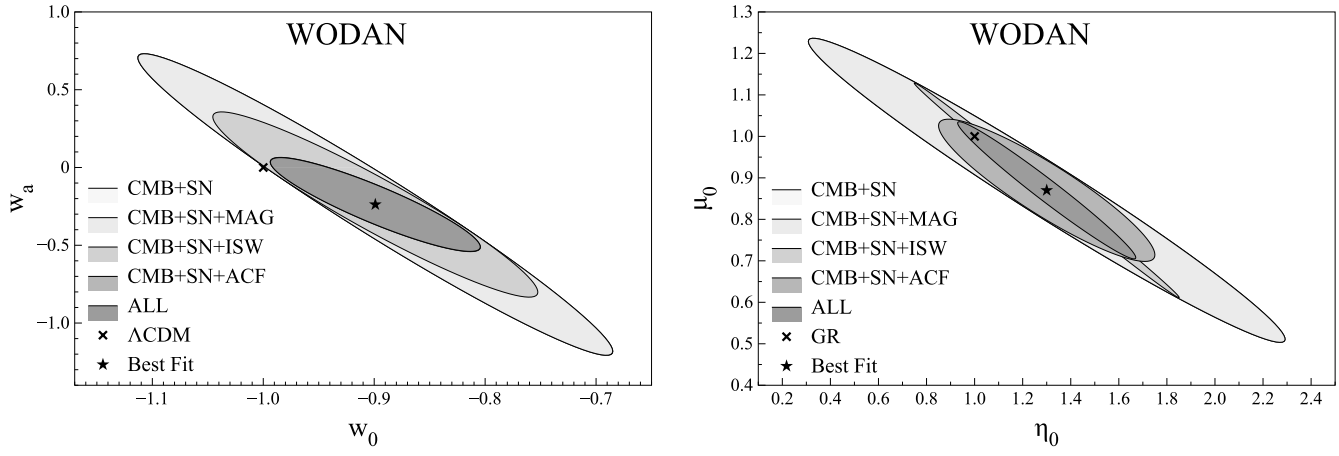


**Figure 14.** Forecast of constraints for the dark energy (left) and modified gravity (right) parameters, for the WODAN survey. Ellipses show $1\sigma$ constraints for different combinations of probes (see text for details). Some probes give very similar errors, so all five ellipses are not always visible.

We use the best-fitting model $\{w_0, w_a\} = \{-0.89, -0.24\}$ from current data (for details, see Zhao & Zhang 2010) as the fiducial model, which is consistent with the prediction of the quintom model (Feng, Wang & Zhang 2005) and consistently includes the dark energy perturbations in the calculation using the prescription proposed in Zhao et al. (2005).

### 6.2 Modified gravity

An intriguing alternative to dark energy as an explanation for the accelerated expansion of the Universe is the modified gravity approach (Durrer & Maartens 2008). This theory states that gravity needs to be modified (i.e. weakened on large scales). An attractive

feature of modified gravity models is that it is possible to alter the Einstein–Hilbert action so that accelerated solutions of the background of the Universe can be obtained without the need for a dark energy component.

In this case, we modify the geometric side of equation (35):

$$G_{\mu\nu} + G^{\rm dark}_{\mu\nu} = T_{\mu\nu}. \tag{40}$$

Modified gravity models can mimic the ΛCDM model, in the sense that they include the background expansion, but in general they predict different dynamics for the growth of cosmic structures. Radio-source number counts and ISW measurements directly probe structure formation, and therefore they can constrain modified gravity scenarios.

Here, we follow Zhao et al. (2010) in considering scalar metric perturbations around a Friedmann–Robertson–Walker (FRW) background, for which the line element in the conformal Newtonian gauge is

$$\mathrm{d}s^2 = -a^2(\tau)\left[(1+2\Psi)\,\mathrm{d}\tau^2 - (1-2\Phi)\,\mathrm{d}\boldsymbol{x}^2\right], \tag{41}$$

where Φ and Ψ are both functions of time and space.

We use the following parametrization to describe the relations specifying how the metric perturbations relate to each other, and how they are sourced by the perturbations of the energy-momentum tensor:

$$\frac{\Phi}{\Psi} = \eta(a,k); \tag{42}$$

$$\Psi = \frac{-4\pi G a^2 \mu(a,k)\varrho\Delta}{k^2}. \tag{43}$$

Here, Δ is the gauge-invariant comoving density contrast, defined as

$$\Delta \equiv \delta + 3\frac{aH}{k}v, \tag{44}$$

and $\eta(a,k)$ and $\mu(a,k)$ are two time- and scale-dependent functions encoding the modifications of gravity, which can be written as

$$\eta(a,k) = \frac{1+\beta_1\lambda_1^2k^2a^{\rm s}}{1+\lambda_1^2k^2a^{\rm s}} \tag{45}$$

and

$$\mu(a,k) = \frac{1+\beta_2\lambda_2^2k^2a^{\rm s}}{1+\lambda_2^2k^2a^{\rm s}}. \tag{46}$$

Here, $\lambda_i^2$ and $\beta_i$ are parameters and $a^{\rm s}$ gives the time dependence of the deviation from GR; $\eta(a,k) = \mu(a,k) = 1$ in GR, while in a modified gravity model $\mu$ and $\eta$ can, in general, be functions of both time and scale (Bertschinger & Zukin 2008; Zhao et al. 2009; Linder 2011).

Because we are interested in testing GR at late times, we consider a simple approximation to equations (45) and (46) where we assume $\mu(a,k) = \eta(a,k) = 1$ at early times, with a transition to some other values at late times. This is natural in the existing models of modified gravity, which aim to explain the late-time acceleration, where departures from GR occur at around the present-day horizon scales. Also, the success in explaining the big bang nucleosynthesis and CMB physics relies on GR being valid at high redshifts.

To model the time evolution of $\mu$ and $\eta$, we use the hyperbolic tangent function to describe the transition from unity to the constants $\mu_0$ and $\eta_0$:

$$\mu(z) = \frac{1-\mu_0}{2}\left(1+\tanh\frac{z-z_{\rm s}}{\Delta z}\right) + \mu_0, \tag{47}$$

$$\eta(z) = \frac{1-\eta_0}{2}\left(1+\tanh\frac{z-z_{\rm s}}{\Delta z}\right) + \eta_0. \tag{48}$$

Here, $z_{\rm s}$ denotes the threshold redshift where we start to modify gravity and $\mu_0$ and $\eta_0$ are free parameters. Following Zhao et al. (2010), we fix the transition width $\Delta z$ to be 0.05.

### 6.3 Observables and Fisher matrices

We use the observables, including the LOFAR, EMU and WODAN radio-source autocorrelation $C_\ell^{gg}$, the cross-correlation $C_\ell^{gT}$ and the magnification bias $C_\ell^{g\mu}$ functions, in a Fisher analysis. To obtain the autocorrelation functions, we consider radio-source-predicted distributions for LOFAR, EMU and WODAN. For the ISW signal, we cross-correlate the radio-source distributions with the CMB, while to obtain the magnification correlations we use SDSS DR7 and DES galaxy populations as foreground lenses for the Northern and Southern hemispheres, respectively. The two-point functions we use can be generalized as

$$C_\ell^{XY} = 4\pi\int\frac{\mathrm{d}k}{k}\Delta^2(k)W_\ell^X(k)W_\ell^Y(k), \tag{49}$$

where $\Delta^2(k)$ is the power spectrum and $W_\ell^{X,Y}(k)$ denote angular window functions. Here, $X, Y \in [T, g, \mu]$, where $T$, $g$ and $\mu$ indicate the CMB temperature, radio-source counts and magnification, respectively.

Given the specifications of the proposed future surveys, the Fisher matrix (Fisher 1935; Tegmark, Taylor & Heavens 1997) enables us to quickly estimate the errors on the cosmological parameters around the fiducial values. For Gaussian-distributed observables, such as $C_\ell^{XY}$, the Fisher matrix is given by

$$F_{\alpha\beta} = f_{\rm sky}\sum_{\ell=\ell_{\rm min}}^{\ell_{\rm max}}\frac{2\ell+1}{2}\mathrm{Tr}\left(\frac{\partial\boldsymbol{C}_\ell}{\partial p_\alpha}\tilde{\boldsymbol{C}}_\ell^{-1}\frac{\partial\boldsymbol{C}_\ell}{\partial p_\beta}\tilde{\boldsymbol{C}}_\ell^{-1}\right), \tag{50}$$

where $p_{\alpha(\beta)}$ is the $\alpha(\beta)$th cosmological parameter and $\tilde{\boldsymbol{C}}_\ell$ is the observed covariance matrix with elements $\tilde{C}_\ell^{XY}$, which include contributions from noise:

$$\tilde{C}_\ell^{XY} = C_\ell^{XY} + N_\ell^{XY}. \tag{51}$$

Equation (50) assumes that all fields $X(\hat{\boldsymbol{n}})$ are measured over contiguous regions covering a fraction $f_{\rm sky}$ of the sky. The value of the lowest multipole can be estimated from $\ell_{\rm min} \approx [\pi/(2f_{\rm sky})]$, where the square brackets denote the rounded integer. For the noise matrix $N_\ell^{XY}$, we use equations (31), (32) and (34).

To perform the Fisher analysis, we first parametrize our cosmology using

$$\boldsymbol{P} \equiv (\omega_{\rm b}, \omega_{\rm c}, \Theta_{\rm s}, \tau, n_{\rm s}, A_{\rm s}, \aleph, \beth), \tag{52}$$

where $\omega_{\rm b} \equiv \Omega_{\rm b}h^2$ and $\omega_{\rm c} \equiv \Omega_{\rm c}h^2$ are the physical baryon and CDM densities, respectively, relative to the critical density, $\Theta_{\rm s}$ is the ratio (multiplied by 100) of the sound horizon to the angular diameter distance at decoupling, $\tau$ denotes the optical depth to reionization, $n_{\rm s}$ and $A_{\rm s}$ are the primordial power spectrum index and amplitude, respectively, and $\aleph \in [w_0, \eta_0]$ and $\beth \in [w_a, \mu_0]$ are the parameters we want to measure. We assume a flat Universe and an effective dark energy equation of state $w = -1$ throughout the expansion history. We also combine the latest Type Ia supernovae (SNe Ia) luminosity distance from the UNION2 sample (Amanullah et al. 2010) in order to tighten the constraints.

Finally, given the uncertainties in the measurement of the bias and the redshift distribution for radio surveys, we marginalize over

the amplitude of the product $b(z) \times N(z)$. We note that the models we use are constrained by the total number of radio-source counts and our current knowledge of the evolution of the subpopulations. The main uncertainties in these distributions is in the high-redshift ($z > 1$) evolution of the FR I radio galaxies (e.g. Clewley & Jarvis 2004; Sadler et al. 2007). However, rapid progress on pinning down the evolution of these source should be made over the next few years by combining deep multiwavelength survey data with deep radio continuum data (e.g. Smolčić et al. 2009; McAlpine & Jarvis 2011). The final results also depend on the shape of this product, which is not precisely known. However, we have verified that modifications at the level of a few per cent in the peak position, amplitude or width do not significantly affect our results. A complete analysis of the impact of this uncertainty on the measurement of cosmological parameters is beyond the scope of this paper, and this is left for future work. Of course, a careful treatment of this issue will be required in the real data analyses, as we have mentioned in Section 8.1.

We use MGCAMB (Zhao et al. 2009)[7] to calculate the observables in modified gravity for LOFAR, EMU and WODAN, and we use equation (50) to calculate the Fisher matrices, using the preferred model of current data as a fiducial model. Following Zhao et al. (2009, 2010), we assume as fiducial $\{w_0, w_a\} = \{-0.89, -0.24\}$ for the dynamical dark energy parameters and $\{\eta_0, \mu_0\} = \{1.3, 0.87\}$ for the modified gravity parameters.

## 7 RESULTS

The results of our forecasts are shown in Figs 11–14. We plot the limits that it will be possible to obtain, using the surveys considered, in the measurements of the dynamical dark energy and modified gravity parameters. To highlight the constraining ability of different observables, we show the contours for different data combinations. The lighter grey areas are limits from the *Planck* CMB[8] plus SNe Ia measurements (Amanullah et al. 2010), while the darker grey areas are improvements we will make by adding the autocorrelation of radio sources, the radio-source–CMB cross-correlation (ISW), the foreground galaxy–background radio-source cross-correlation (cosmic magnification) and a combination of all the measurements. The crosses refer to the standard model (cosmological constant and GR) and stars indicate the current best fit from a combination of probes using *WMAP*, SDSS and CFHTLS (for details, see Zhao et al. 2010).

We can see that the precision in the measurements of cosmological parameters will be significantly increased by the addition of the probes considered. In particular, we note that the ISW effect is more powerful in testing models for gravity than models of dark energy. If it turns out that gravity needs to be modified, the ISW effect measured with radio surveys will be a powerful probe to measure the modified gravity parameters. The physical reason for this is that if $\mu_0$ transits from 1 to another value at low $z$, indicating a deviation from GR, the growth will be enhanced. This will change $(\dot{\Phi} + \dot{\Psi})$ significantly, hence generating a large ISW signal (equation 13).

Analyses of clustering and magnification bias also tighten the constraints on gravity. The magnification signal measures information about the power spectrum of $(\Phi + \Psi)$, which is largely controlled by $\eta_0$, and it also tests $\mu_0$ via the growth of structures. The ACF is also sensitive to $\mu_0$ for this reason. These probes will also be useful in measuring the parameters of the dark energy component, if GR is correct even at the largest scales. This is because $w(a)$ changes the growth in a very smooth way. So, while it does not generate a large ISW signal, it does change the $(\Phi + \Psi)$ power integrated along the line of sight, as can be seen by the magnification bias and the projected ACF.

Looking at the different surveys, we can see that they will allow precise measurements of cosmological parameters. LOFAR Tier1, EMU and WODAN should all be able to increase, by a significant amount, the precision in the dark energy and modified gravity measurements, compared with that predicted for CMB+SNe. It is also interesting to note that the addition of measurements from LOFAR MS[3], which is the least powerful of the surveys we have considered (because of the lower number density of sources), will decrease the errors in the measurements on modified gravity parameters with respect to those of CMB+SN Ia.

Finally, Fig. 15 shows the constraints on the parameters of dynamical dark energy and modified gravity that can be obtained by using the combination of EMU and WODAN. We compare these to the current best measurements available (Zhao et al. 2010). We see that there is a substantial improvement, which we quantify in Table 2, where we report the limits on the measurements of the four parameters for the different techniques using the single surveys and the EMU+WODAN combination.

## 8 DISCUSSION AND CONCLUSIONS

In this paper, we have presented a forecast of the cosmological measurements that will be possible with data from the forthcoming LOFAR, EMU and WODAN radio surveys. We have used the correlation spectra of radio sources (i.e. the autocorrelation, the correlations with the CMB and with foreground galaxies, alone and in combination) to predict measurements of cosmological parameters.

As mentioned in Section 3.1, the EMU and WODAN surveys can be combined to obtain a complete full-sky catalogue, and thus the largest possible sky coverage. Fig. 15 shows the improvements that this combination will produce when constraining cosmological parameters. However, this combination and all the measurements we have highlighted will require a very careful treatment of observational data and systematic errors. Future work will concentrate on a detailed analysis of these issues.

### 8.1 Implications for survey design

The tests described in this paper will be very sensitive to systematic errors. For example, in order to measure magnification bias, it is necessary for the background source samples to be uniformly surveyed (or for the threshold variation and completeness to be well understood) over large areas, which places a stringent requirement on the flux calibration of the surveys. Systematics such as these lead to a number of requirements on the surveys, and here we make some initial comments about the nature of these requirements.

(i) Uniformity and completeness. It is important that the tests described in this paper are conducted either on a uniform sample, or on one where fluctuations are well understood. For instance, a uniform sample can be created by imposing a flux-density cut that is sufficiently above the sensitivity limit at the most insensitive part of the survey, so that there are few spurious sources, and so that sources are not lost to systematic effects. Detailed simulations will be necessary to check the impact of the flux threshold, given the consequent non-uniform signal-to-noise.

[7] http://zhaog.myweb.port.ac.uk/MGCAMB.html
[8] http://www.rssd.esa.int/index.php?project=planck

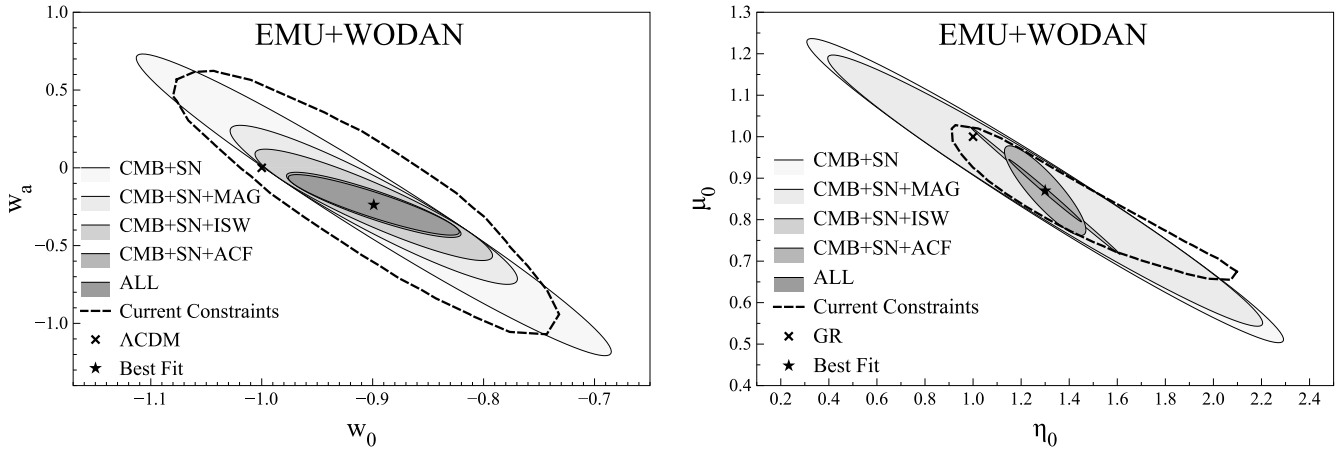


**Figure 15.** Forecast of constraints on the dynamical dark energy (left) and modified gravity (right) parameters with the EMU+WODAN combination, for different combinations of probes (grey shaded areas), compared with current measurements (solid dashed lines). Some probes give very similar errors, so all five ellipses are not always visible.

(ii) Calibration accuracy of individual surveys. Most surveys typically aim for a 1 per cent calibration accuracy. It will be important to try to maintain this level because of the need for uniformity described above, and because of the problems that arise if these calibration errors occur systematically and not randomly across the field.

(iii) Dynamic range. If a strong radio source causes low-level artefacts, then these will affect the claimed number of faint (and therefore typically distant) galaxies, resulting in a spurious correlation between low-redshift and high-redshift galaxies. To first order, this will be seen as an increase in rms map noise towards bright sources. Any cosmic measurements need to take this into account, possibly by masking the affected area, with the consequence of reducing the sky-coverage slightly.

(iv) Cross-calibration of different surveys. It would be useful for all of the surveys to overlap in some regions of the sky in order to ensure an accurate absolute flux scale.

(v) Large-scale gradients, especially in the declination direction, are virtually unavoidable because of changing ultraviolet coverage as a function of declination and increased system temperatures for low elevation observations. These need to be carefully corrected.

(vi) Bias and redshift distribution uncertainties. This is a well-known issue for both the galaxy–galaxy and galaxy–CMB temperature spectra and for the redshift distribution only for cosmic magnification. While there have recently been several attempts to model the bias in a more accurate way, we have used the models of Wilman et al. (2008) for consistency with the redshift distribution models. To take this uncertainty into account, we marginalized over the amplitude of $b(z) \times N(z)$ (see Section 6.3 for more details). A reliable measurement of redshift and bias for the radio continuum population will allow us to improve the constraining power of the techniques considered in this paper. This is the subject of a future paper (Lindsay, in preparation).

### 8.2 Additional measurements

In addition to the techniques presented in this paper, the LOFAR, EMU and WODAN data will enable several other cosmological analyses, which will be useful for testing and improving our models. As examples, we briefly mention two interesting possibilities: the measurement of a dipole anisotropy and a study of the CMB cold spot.

The measurement of a dipole anisotropy in the distribution of radio sources can be used to test the distribution of matter at different distances and to constrain our local motion with respect to the comoving cosmic rest frame.

The dipole anisotropy in the CMB has been detected with good precision, so an accurate measurement of the dipole anisotropy in the large-scale mass distribution at lower redshift will allow a test of the homogeneity of the matter distribution in the Universe. If there is agreement between the dipole in the CMB and the dipole of galaxies, this will suggest a large-scale homogeneity, while a discrepancy between the CMB and the nearby dipole would cast doubt on the general assumption of isotropy and homogeneity of the Universe on large scales.

It is valuable to have radio sky surveys at different frequencies (e.g. LOFAR and WODAN), because the amplitude of the radio dipole is a function not only of our peculiar velocity, but also of the spectral index of radio emission (Ellis & Baldwin 1984).

A detection of the dipole anisotropy in the radio-source distribution has been reported using NVSS (Blake & Wall 2002), but the significance of this measurement depends strongly on the number of sources. The surveys considered here will provide an impressive improvement in the precision of the dipole anisotropy measurement, because they will be able to move from an uncertainty of $\sim 15^\circ$ in the dipole direction (Blake & Wall 2002), to an improved accuracy of $\sim 2^\circ$ at the $1\sigma$ level (Crawford 2009).

Using the radio-source distribution, it will also be possible to perform a number count analysis in order to search for a void in the direction of the cold spot (Cruz et al. 2005) in the CMB. Several models have been proposed to explain this anomaly, for example, voids (Inoue & Silk 2006; Rudnick 2007), second-order gravitational effects (Tomita & Inoue 2008) or a brane-world model (Cembranos et al. 2008). Using a Bayesian statistical analysis, Cruz et al. (2007) have shown that the cosmic texture explanation is favoured over the Rees–Sciama effect (Rees & Sciama 1968) because of a void or the Sunyaev–Zel'dovich effect (Zel'dovich & Sunyaev 1969) caused by a cluster. Radio and optical data have been used to test the void hypothesis (Bremer et al. 2010; Granett, Szapudi & Neyrinck 2010), in an attempt to find a gap in the number density in the direction of the cold spot. No gap was found, but a further analysis using the EMU survey will be helpful, because the larger number density of sources at high redshifts will provide much better signal-to-noise ratio for a potential void. Such an anomalously

large void will also leave an imprint on ISW measurements (Granett, Neyrinck & Szapudi 2008), and again this can be examined using EMU data.

### 8.3 Conclusions

In this paper, we have shown the potential of SKA pathfinder-generation radio surveys to provide competitive cosmological measurements that are able to test cosmological models and to constrain the parameters describing fundamental physics models.

Using simulated catalogues, we have predicted which measurements we will obtain with the source autocorrelation, the cross-correlation between sources and the CMB, the magnification bias, and a joint analysis together with the CMB power spectrum and SNe Ia.

We have shown examples of the constraining power in testing alternative cosmological models to the ΛCDM+GR model, looking for modifications coming from non-Gaussianity, alternative models for dark energy or modifications to the theory of gravity. We have assumed that the surveys will achieve their target data set and treatment of systematic errors, but we have tried to be conservative in our analyses (e.g. marginalizing over the amplitude of correlation power spectra, and using objects detected at the $10\sigma$ signal-to-noise threshold).

There are a number of other galaxy surveys at different wavelengths that aim to measure cosmological parameters, which are already collecting data or are being actively prepared for. The radio surveys discussed in this paper are complementary to these surveys, because of the difference in area, redshift and number density covered, and so they will be able to provide useful information using some specific probes (i.e. ISW and cosmic magnification, because their constraining power is increased for larger sky coverage and higher redshifts). In the period before SKA, three-dimensional redshift surveys, such as the Baryon Oscillation Spectroscopic Survey (BOSS), will provide more information on the power spectrum on intermediate scales and at low redshifts. Photometric surveys, such as Pan-STARRS1[9] and DES, will also span a different part of the parameter space, because they will observe a larger number of objects, but at a lower median redshift and, in some cases, for a smaller region of the sky. Radio surveys cover larger volumes, and so provide more large-scale information. Thus, they will be complementary to these other surveys. Next-generation experiments, such as Euclid and the LSST, will improve the quality of available data but, for some aspects, the radio surveys of the current generation are still competitive, as can be seen from Fig. 16. NVSS has been used to perform radio cosmological analyses (e.g. Raccanelli et al. (2008), Xia et al. (2010a)). The surveys we have considered here will have a higher median redshift and a higher number of objects observed, so they should improve the precision of the cosmological measurements available.

Our results show that the unprecedented combination of sky coverage, redshift range and sensitivity will enable high-precision measurements, competitive with current surveys in a conservative scenario. By examining Fig. 15 and Table 2, it is clear that the measurements that LOFAR, EMU and WODAN could provide are potentially decisive in ruling out a large part of the cosmological parameter space for dark energy and modified gravity models.

[9] The parameters are from Baugh (2008).

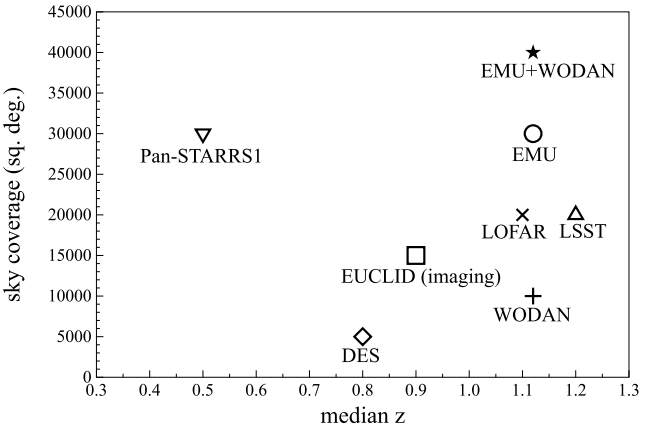


**Figure 16.** Comparison of median redshift and sky coverage of selected future imaging surveys.

**Table 2.** Errors on the measurements of dark energy and modified gravity parameters for the different surveys and probe combinations. The current best measurements are $\{w_0, w_a\} = \{-0.89 \pm 0.11, -0.24 \pm 0.56\}$ (Zhao & Zhang 2010) and $\{\eta_0, \mu_0\} = \{1.3 \pm 0.35, 0.87 \pm 0.12\}$ (Zhao et al. 2010).

| Probe | $\sigma_{w_0}$ | $\sigma_{w_a}$ | $\sigma_{\eta_0}$ | $\sigma_{\mu_0}$ |
|---|---|---|---|---|
| CMB + SNe | 0.14 | 0.64 | 0.66 | 0.24 |
| CMB + SNe + LOFAR MS$^3$ ISW | 0.13 | 0.59 | 0.38 | 0.18 |
| CMB + SNe + LOFAR MS$^3$ ACF | 0.12 | 0.51 | 0.64 | 0.23 |
| CMB + SNe + LOFAR MS$^3$ MAG | 0.14 | 0.64 | 0.66 | 0.24 |
| CMB + SNe + LOFAR MS$^3$ ALL | 0.14 | 0.49 | 0.38 | 0.17 |
| CMB + SNe + LOFAR Tier1 ISW | 0.11 | 0.51 | 0.35 | 0.16 |
| CMB + SNe + LOFAR Tier1 ACF | 0.07 | 0.29 | 0.54 | 0.19 |
| CMB + SNe + LOFAR Tier1 MAG | 0.14 | 0.64 | 0.66 | 0.24 |
| CMB + SNe + LOFAR Tier1 ALL | 0.07 | 0.28 | 0.32 | 0.14 |
| CMB + SNe + EMU ISW | 0.07 | 0.25 | 0.22 | 0.11 |
| CMB + SNe + EMU ACF | 0.05 | 0.14 | 0.11 | 0.07 |
| CMB + SNe + EMU MAG | 0.08 | 0.34 | 0.60 | 0.21 |
| CMB + SNe + EMU ALL | 0.05 | 0.13 | 0.10 | 0.05 |
| CMB + SNe + WODAN ISW | 0.09 | 0.39 | 0.36 | 0.16 |
| CMB + SNe + WODAN ACF | 0.06 | 0.20 | 0.30 | 0.11 |
| CMB + SNe + WODAN MAG | 0.14 | 0.64 | 0.66 | 0.24 |
| CMB + SNe + WODAN ALL | 0.06 | 0.20 | 0.24 | 0.11 |
| CMB + SNe + EMU+WODAN ISW | 0.07 | 0.23 | 0.20 | 0.10 |
| CMB + SNe + EMU+WODAN ACF | 0.05 | 0.13 | 0.11 | 0.07 |
| CMB + SNe + EMU+WODAN MAG | 0.08 | 0.34 | 0.60 | 0.21 |
| CMB + SNe + EMU+WODAN ALL | 0.05 | 0.12 | 0.10 | 0.05 |

## ACKNOWLEDGMENTS

AR is grateful for the support from a UK Science and Technology Facilities Research Council (STFC) PhD studentship. GBZ is supported by STFC grant ST/H002774/1. Both DB and MJJ acknowledge support from Research Councils UK fellowships. WJP is grateful for support from the European Research Council, the Leverhulme Trust and STFC. DJS acknowledges financial support from the Deutsche Forschungsgemeinschaft (DFG). We thank Daniele Bertacca, Emma Beynon, Annalisa Bonafede, Rob Crittenden, Olivier Doré, Tommaso Giannantonio, Ben Hoyle, Minh Huynh, Joseph Lazio, Alejo Martinez-Sansigre, Sabino Matarrese, Matthias Rubart, Hana Schumacher, Charles Shapiro, David Wands and Jun-Qing Xia for valuable discussions. Numerical computations were carried out on the SCIAMA High Performance Compute

(HPC) cluster, which is supported by the Institute of Cosmology and Gravitation (ICG), the South East Physics Network (SEPNet) and the University of Portsmouth.

## REFERENCES

Abazajian K. N. et al., 2009, ApJS, 182, 543
Abdalla F. B., Rawlings S., 2005, MNRAS, 360, 27
Abdalla F. B., Blake C., Rawlings S., 2010, MNRAS, 401, 743
Amanullah R. et al., 2010, ApJ, 716, 712
Bartelmann M., Schneider P., 2001, Phys. Rep., 340, 291
Bartolo N., Komatsu E., Matarrese S., Riotto A., 2004, Phys. Rep., 402, 103
Baugh C. M., 2008, Phil. Trans. R. Soc. A, 366 (1884), 4381
Becker R. H., White R. L., Helfand D. J., 1995, AJ, 112, 407
Bennett C. L. et al., 2011, ApJS, 192, 17
Bertacca D., Bartolo N., Diaferio A., Matarrese S., 2008, JCAP, 10, 023
Bertacca D., Raccanelli A., Piattella O., Pietrobon D., Bartolo N., Matarrese S., Giannantonio T., 2011, JCAP, 03, 039
Bertschinger E., Zukin P., 2008, Phys. Rev. D, 78, 024015
Bessel F., 1824, Abh. d. K. Akad. Wiss. Berlin, 1
Blake C., Wall J., 2002, Nat, 416, 150
Boughn S., Crittenden R., 2002, Phys. Rev. D, 88, 021302
Boughn S., Crittenden R., 2004, Nat, 427, 45
Bremer M. N., Silk J., Davies L. J. M., Lehnert M. D., 2010, MNRAS, 404, L69
Cabre A., Fosalba P., Gaztanaga E., Manera M., 2007, MNRAS, 381, 1347
Cembranos J. A. R., de la Cruz-Dombriz A., Dobado A., Maroto A. L., 2008, JCAP, 10, 039
Clewley L., Jarvis M. J., 2004, MNRAS, 352, 909
Cole S., Kaiser N., 1989, MNRAS, 237, 1127
Condon J., Cotton W. D., Greisen E. W., Yin Q. F., Perley R. A., Taylor G. B., Broderick J. J., 1998, AJ, 115, 1693
Copi C. J., Huterer D., Schwarz D. J., Starkman G. D., 2010, Adv. Astron., 2010, 847541
Crawford F., 2009, ApJ, 692, 887
Crittenden R. G., Turok N., 1996, Phys. Rev. Lett., 76, 575
Cruz M., Martinez-Gonzalez E., Vielva P., Cayon L., 2005, MNRAS, 356, 29
Cruz M., Turok N., Vielva P., Martinez-Gonzalez E., Hobson M., 2007, Sci, 318, 1612
Dalal N., Doré O., Huterer D., Shirokov A., 2008, Phys. Rev. D, 77, 123514
Desjacques V., Seljak U., 2010, Class. Quant. Grav., 27, 124011
Dupe F. X., Rassat A., Starck J. L., Fadili M. J., 2010, A&A, 534, A51
Durrer R., Maartens R., 2008, Gen. Rel. Grav., 40, 301
Eisenstein D. et al., 2011, AJ, 142, 72
Ellis G. F. R., Baldwin J. E., 1984, MNRAS, 206, 377
Feng B., Wang X., Zhang X., 2005, Phys. Lett. B, 607, 35
Fisher R. A., 1935, J. R. Stat. Soc., 98, 39
Giannantonio T. et al., 2006, Phys. Rev. D, 74, 063520
Giannantonio T., Scranton R., Crittenden R. G., Nichol R. C., Boughn S. P., Myers A. D., Richards G. T., 2008a, Phys. Rev. D, 77, 12
Giannantonio T., Song Y-S., Koyama K., 2008b, Phys. Rev. D, 78, 044017
Granett B. R., Neyrinck M. C., Szapudi I., 2008, ApJ, 683, L99
Granett B. R., Szapudi I., Neyrinck M. C., 2010, ApJ, 714, 825
Hamilton A. J. S., 1993, ApJ, 417, 19
Hildebrandt H., van Waerbeke L., Erben T., 2009, A&A, 507, 683
Ho S., Hirata C., Padmanabhan N., Seljak U., Bahcall N., 2008, Phys. Rev. D, 78, 043519
Inoue K. T., Silk J., 2006, ApJ, 648, 23
Johnston S. et al., 2008, Exp. Astron., 22, 151
Jonas J., 2009, in Heald G., Serra P., eds, Proceedings of Science, SISSA, Article No. 4
Kaiser N. et al., 2010, Proc. SPIE, 7733, 12
Kazin E. et al., 2010, ApJ, 710, 1444
Komatsu E., 2010, Class. Quantum Grav., 27, 124010
Komatsu E., et al, 2011, ApJS, 192, 18
Landy S. D., Szalay A. S., 1993, ApJ, 412, 64
Laureijs R., 2009, preprint (arXiv:0912.0914)
Legendre A. M., 1785, Mém. Math. Phys., 10, 411
Linder E. V., 2003, Phys. Rev. Lett., 90, 091301
Linder E. V., 2011, Phil. Trans. R. Soc. A, 369, 4985
Loverde M., Hui L., Gaztañaga E., 2007, Phys. Rev. D, 75, 043519
McAlpine K., Jarvis M. J., 2011, MNRAS, 413, 1054
Massardi M., Bonaldi A., Negrello M., Ricciardi S., Raccanelli A., De Zotti G., 2010, MNRAS, 404, 532
Matarrese S., Coles P., Lucchin F., Moscardini L., 1997, MNRAS, 286, 115
Matarrese S., Verde L., Jimenez R., 2000, ApJ, 541, 10
Ménard B., Scranton R., Fukugita M., Richards G., 2010, MNRAS, 405, 1025
Mo H. J., White S. D. M., 1996, MNRAS, 282, 347
Morganti R. et al., 2009, in Heald G., Serra P., eds, Proceedings of Science, SISSA, Article No. 40 (arXiv:1001.2384v1)
Moscardini L., Coles P., Lucchin F., Matarrese S., 1998, MNRAS, 299, 95
Norris R. P. et al., 2011, PASA, 28, 215
Oosterloo T., Verheijen M., van Cappellen W., 2010, in Proc. ISKAF2010 Science Meeting, PoS(ISKAF2010). Proceedings of Science, SISSA. http://adsabs.harvard.edu/abs/2010iska.meetE.430
Peebles P. J. E., 1980, The Large-Scale Structure of the Universe. Princeton University Press, Princeton, NJ
Pietrobon D., Balbi A., Marinucci D., 2006, Phys. Rev. D, 74, 043524
Pogosian L., Corasaniti P.-S., Stephan-Otto C., Crittenden R., Nichol R., 2005, Phys. Rev. D, 72, 103519
Press W., Schechter P., 1974, ApJ, 187, 425
Raccanelli A., Bonaldi A., Negrello M., Matarrese S., Tormen G., de Zotti G., 2008, MNRAS, 386, 2161
Rassat A., 2009, preprint (arXiv:0902.1759)
Rees M. J., Sciama D. W., 1968, Nat, 217, 511
Ross A. et al., 2011, MNRAS, 417, 1350
Röttgering H. J. A., 2003, New Astron. Rev., 47, 405
Röttgering H. J. A., 2010, in Proc. ISKAF2010 Science Meeting, PoS(ISKAF2010). Proceedings of Science, SISSA, 050. http://pos.sissa.it/cgi-bin/reader/conf.cgi?confid=112
Röttgering H. et al., 2012, J. Astrophys. Astron., in press (doi:10.1007/s12036-011-9129-x)
Rudnick L., Brown S., Williams L., 2007, ApJ, 671, 40
Sachs R. K., Wolfe A. M., 1967, ApJ, 147, 73
Sadler E. M. et al., 2007, MNRAS, 381, 211
Samushia L., Percival W. J., Raccanelli A., 2012, MNRAS, 420, 2102
Schaefer B. M., Douspis M., Aghanim N., 2009, MNRAS, 397, 925
Schlegel D. et al., 2011, preprint (arXiv:1106.1706)
Scranton R. et al., 2005, ApJ, 633, 589
Sheth R. K., Tormen G., 1999, MNRAS, 308, 119
Slosar A., Hirata C., Seljak U., Ho S., Padmanabhan N., 2008, JCAP, 08, 031
Smolčić V. et al., 2009, ApJ, 696, 24
Tegmark M., Taylor A. N., Heavens A. F., 1997, ApJ, 480, 22
Thomas S. A., Abdalla F. B., Lahav O., 2011, Phys. Rev. Lett., 106, 241301
Tomita K., Inoue K. T., 2008, Phys. Rev. D, 77, 103522
Wang L. et al., 2011, MNRAS, 414, 596
Wilman R. J. et al., 2008, MNRAS, 388, 1335
Wilman R. J., Jarvis M. J., Mauch T., Rawlings S., Hickey S., 2010, MNRAS, 405, 447
Xia J-Q., Viel M., Baccigalupi C., Matarrese S., 2009, JCAP, 09, 003
Xia J-Q., Viel M., Baccigalupi C., De Zotti G., Matarrese S., Verde L., 2010a, ApJ, 717, L17
Xia J-Q., Bonaldi A., Baccigalupi C., De Zotti G., Matarrese S., Verde L., Viel M., 2010b, JCAP, 08, 013
Zel'dovich Ya. B., 1967, Zh. Eksp. Teor. Fiz. Pis'ma, 6, 883
Zel'dovich Ya. B., Sunyaev R., 1969, Ap&SS, 4, 301

Zhang P., Pen U. L., 2006, MNRAS, 367, 169
Zhao G-B., Zhang X., 2010, Phys. Rev. D, 81, 043518
Zhao G-B., Xia J. Q., Li M., Feng B., Zhang X., 2005, Phys. Rev. D, 72, 123515
Zhao G-B., Pogosian L., Silvestri A., Zylberberg J., 2009, Phys. Rev. D, 79, 083513
Zhao G-B., Giannantonio T., Pogosian L., Silvestri A., Bacon D. J., Koyama K., Nichol R. C., Song Y-S., 2010, Phys. Rev. D, 81, 103510

This paper has been typeset from a TEX/LATEX file prepared by the author.